Supporting Information

High Affinity Zoledronate-based Metal Complex Nanocrystals to Potentially Treat Osteolytic Metastases

Gabriel Quiñones Vélez[a,b], Lesly Carmona-Sarabia[a,b], Alondra A. Rivera Raíces[b,c], Tony Hu[d], Esther Peterson[c], and Vilmalí López-Mejías[a,b,]*

[a] Department of Chemistry, University of Puerto Rico, Río Piedras
San Juan, Puerto Rico, 00931 United States.
[b] Crystallization Design Institute, Molecular Sciences Research Center,
University of Puerto Rico, San Juan, Puerto Rico, 00926 United States.
[c] Department of Biology, University of Puerto Rico, Río Piedras
San Juan, Puerto Rico, 00931 United States.
[d] Department of Chemistry and the Molecular Design Institute,
New York University, 100 Washington Square East,
New York, New York 10003-6688, United States.

Table of content.

1. Experimental

1.1. Syntheses of ZOLE-based BPCCs

ZOLE-Ca form I. A mixture solution with a molar ratio (1:1) of ZOLE and $Ca(NO_3)_2 \cdot 4H_2O$ was prepared in nanopure water at room temperature as follows. A ligand solution was prepared by dissolving 1 mmol (0.2721 g) of solid ZOLE in 10 mL of nanopure water and heating at 85°C for 2 h. A metal salt solution was prepared dissolving 1 mmol (0.2362 g) of $Ca(NO_3)_2 \cdot 4H_2O$ in 2.5 mL of nanopure water. The metal salt solution was added to the ligand solution with a syringe and mixed thoroughly. The vial was heated at 85°C until crystals appeared (~15 min). The vial was removed from heat and the product was collected by vacuum filtration and air-dried.

ZOLE-Ca form II. A mixture solution with a molar ratio (1:1) of ZOLE and $CaCl_2 \cdot 2H_2O$ was prepared in nanopure water at room temperature as follows. A ligand solution was prepared by dissolving 1 mmol (0.2721 g) of solid ZOLE in 10 mL of nanopure water and heating at 85°C for 2 h. A metal salt solution was prepared dissolving 1 mmol (0.1470 g) of $CaCl_2 \cdot 2H_2O$ in 2.5 mL of nanopure water. The metal salt solution was added to the ligand solution with a syringe and mixed thoroughly. The vial was heated at 85°C until crystals appeared (~1.5 h). The vial was removed from the heat and the product was collected by vacuum filtration and air-dried.

ZOLE-Mg form I. A mixture solution with a molar ratio (1:1:1) of ZOLE, HEDP and $Mg(NO_3)_2 \cdot 6H_2O$ was prepared in nanopure water at room temperature as follows. A ligand solution was prepared by dissolving 1 mmol (0.2721 g) of solid ZOLE and adding 1 mmol (0.23 mL) of aqueous HEDP in 10 mL of nanopure water and heating at 85°C for 2 h. A metal salt solution was prepared dissolving 1 mmol (0.2564 g) of $Mg(NO_3)_2 \cdot 6H_2O$ in 2.5 mL of nanopure water. The metal salt solution was added to the ligand solution with a syringe and mixed thoroughly. The vial was heated at 85°C until crystals appeared (~ 35 min). The vial was removed from heat and the product was collected by vacuum filtration and air-dried.

ZOLE-Mg form II. A mixture solution with a molar ratio (1:1) of ZOLE and $MgCl_2$ was prepared in nanopure water at room temperature as follows. A ligand solution was prepared by dissolving 1 mmol (0.2721 g) of solid ZOLE in 10 mL of nanopure water and heating at 85°C for 2 h. The ligand solution was adjusted with 0.3 M NaOH to reach a pH of ~ 4.0. A metal salt solution was prepared dissolving 1 mmol (0.0952 g) of $MgCl_2$ in 2.5 mL of nanopure water. The metal salt solution was added to the ligand solution with a syringe and mixed thoroughly. The vial was heated at 85°C until crystals appeared (~ 20 min). The vial was removed from heat and the product was collected by vacuum filtration and air-dried.

ZOLE-Zn form I. A mixture solution with a molar ratio (1:1) of ZOLE and $ZnCl_2$ was prepared in nanopure water at room temperature as follows. A ligand solution was prepared by dissolving 1 mmol (0.2721 g) of solid ZOLE in 10 mL of nanopure water and heating at 85°C for 2 h. The metal salt solution was prepared dissolving 1 mmol (0.1363 g) of $ZnCl_2$ in 2.5 mL of nanopure water. The metal solution was added to the ligand solution with a syringe and mixed thoroughly.

The vial was heated at 85°C until prism-like crystals appeared (~1 h). The vial was removed from heat and the product was collected by vacuum filtration and air-dried.

ZOLE-Zn form II. A mixture solution with a molar ratio (1:1) of ZOLE and $ZnCl_2$ was prepared in nanopure water at room temperature as follows. A ligand solution was prepared by dissolving 1 mmol (0.2721 g) of solid ZOLE in 10 mL of nanopure water and heating at 85°C for 2 h. The metal salt solution was prepared dissolving 1 mmol (0.1363 g) of $ZnCl_2$ in 2.5 mL of nanopure water. The metal salt solution was added to the ligand solution with a syringe and mixed thoroughly. The vial was heated at 85°C until prism-like crystals corresponding to ZOLE-Zn form I appeared (~ 1 h). To obtain ZOLE-Zn form II, the solution was removed from heat and left it undisturbed in the bench until needle-like crystals appeared (~ 30 min). This yielded a concomitant mixture of ZOLE-Zn form I (colorless prisms) and II (colorless needles). The product was collected by vacuum filtration and air-dried. The colorless needles corresponding to form II were manually separated from the prisms (ZOLE-Zn form I) for further analysis.

2. Raman Vibrational Spectroscopy

Figures S2.1-S2.6 depict an overlay of the experimental Raman spectra of the ZOLE-based BPCCs and ZOLE.

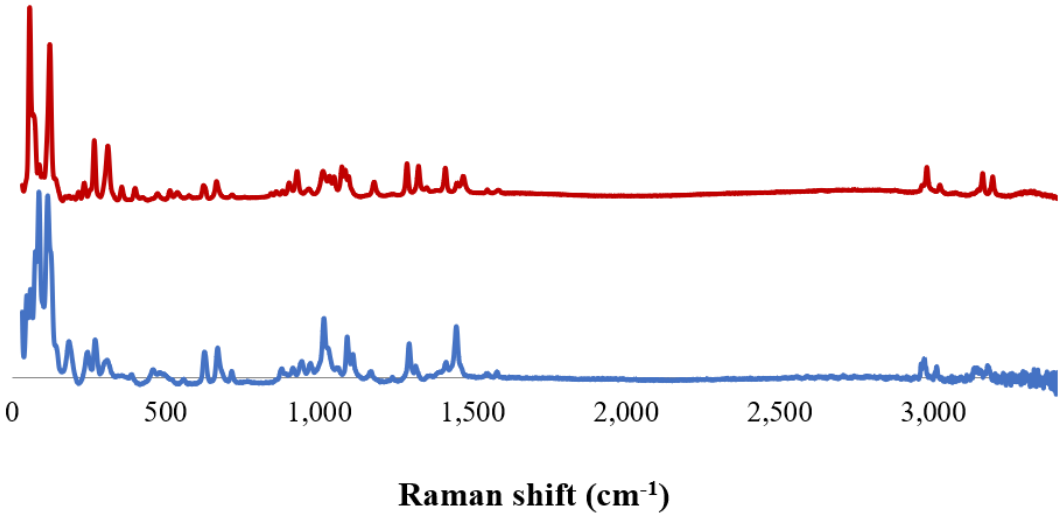

Figure S2.1. Raman spectra overlay of "as received" ZOLE (bottom, blue), and the synthetized ZOLE-Ca form I (top, red).

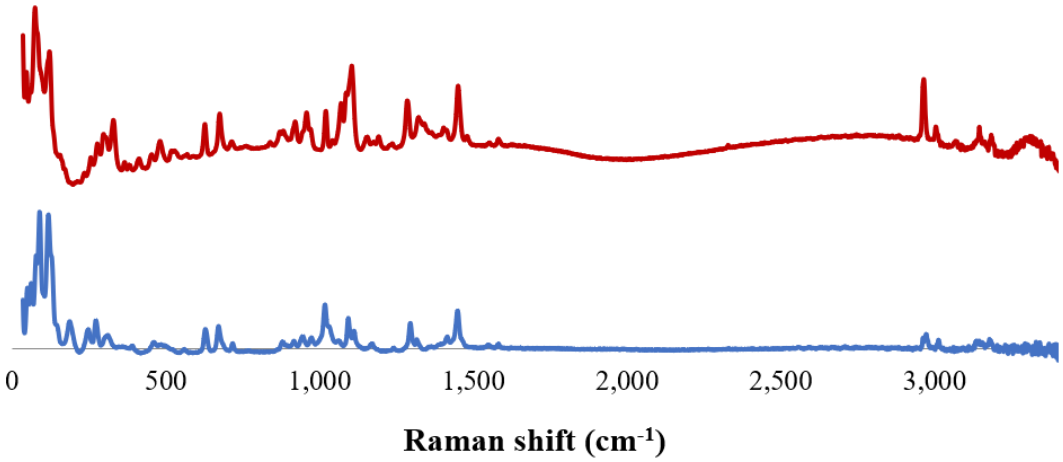

Figure S2.2. Raman spectra overlay of "as received" ZOLE (bottom, blue), and the synthetized ZOLE-Ca form II BPCC (top, red).

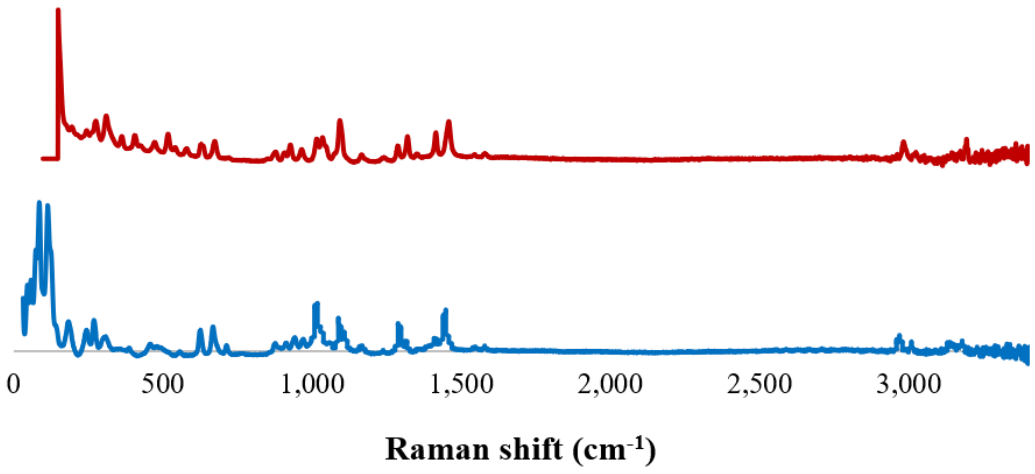

Figure S2.3. Raman spectra overlay of "as received" ZOLE (bottom, blue), and the synthetized ZOLE-Mg form I (top, red).

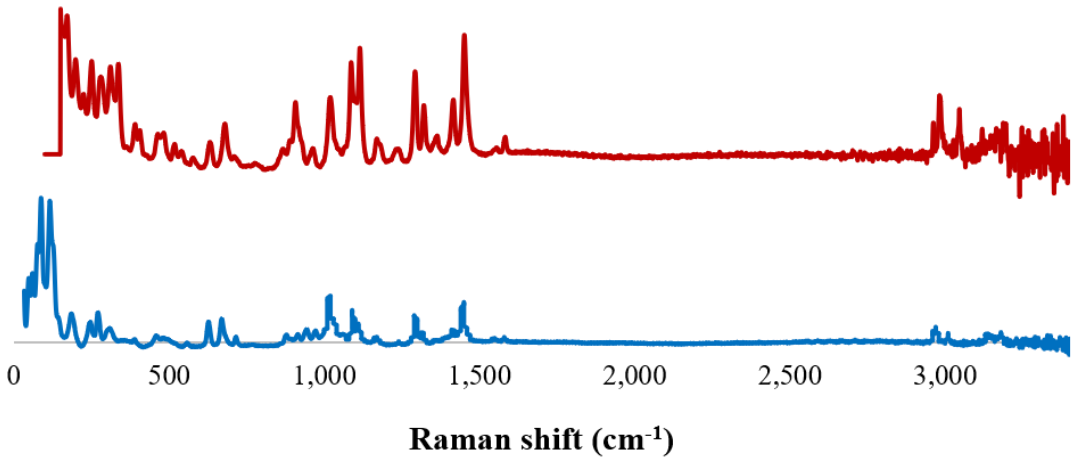

Figure S2.4. Raman spectra overlay of "as received" ZOLE (bottom, blue), and the synthetized ZOLE-Mg form II (top, red).

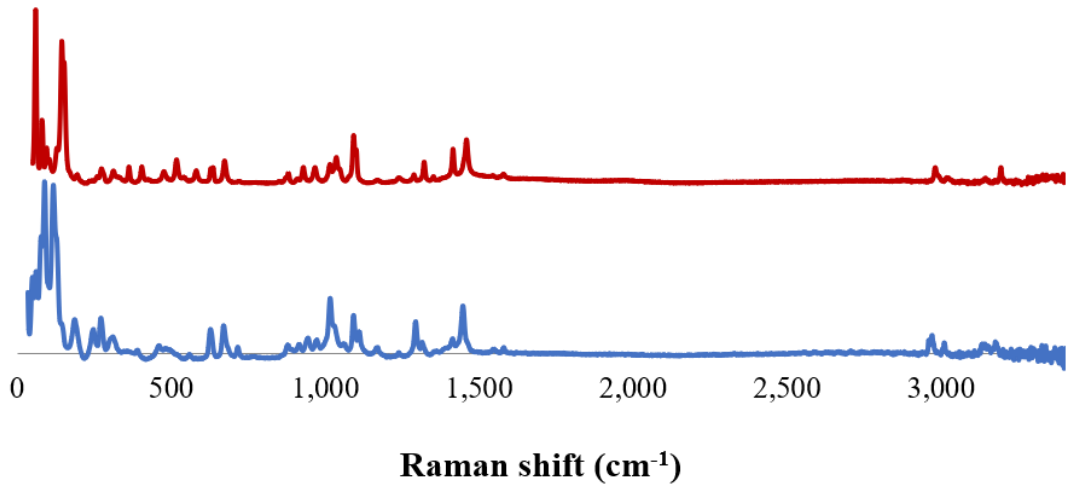

Figure S2.5. Raman spectra overlay of "as received" ZOLE (bottom, blue), and the synthetized ZOLE-Zn form I (top, red).

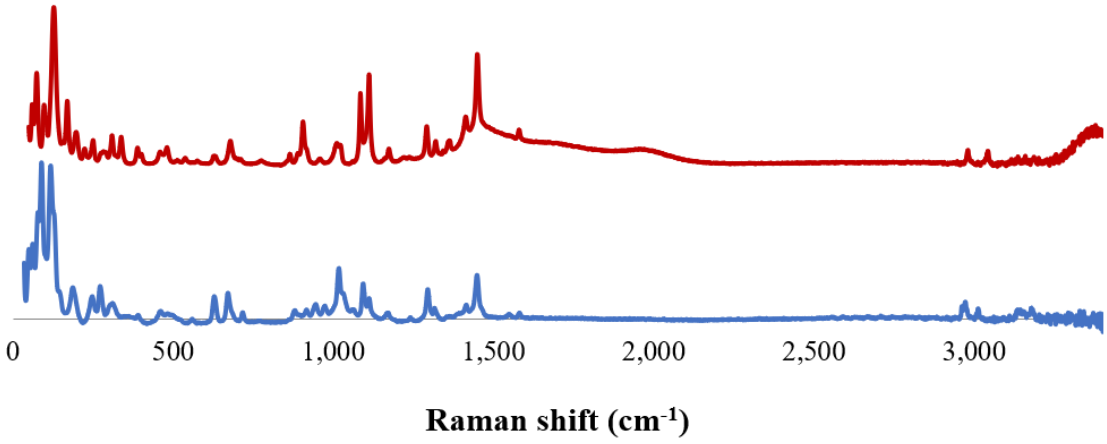

Figure S2.6. Raman spectra overlay of "as received" ZOLE (bottom, blue), and the synthetized ZOLE-Zn form II (top, red).

3. Micro-powder X-ray Diffraction (PXRD)

Figures S3.1-S3.6 depict the experimental powder patterns of the ZOLE-based BPCCs (ZOLE-Ca forms I and II, ZOLE-Mg forms I and II, ZOLE-Zn forms I and II), and ZOLE.

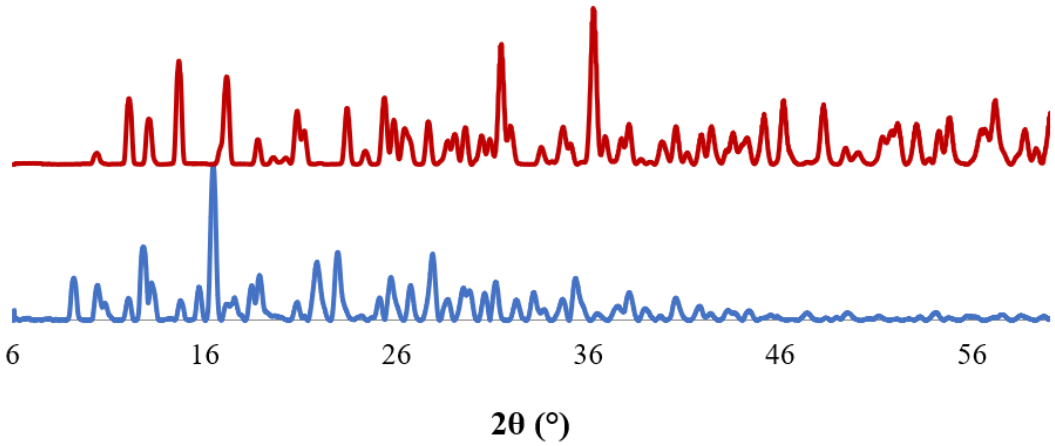

Figure S3.1. Powder X-ray diffractogram overlay of "as received" ZOLE (bottom, blue) and synthetized ZOLE-Ca form I (top, red).

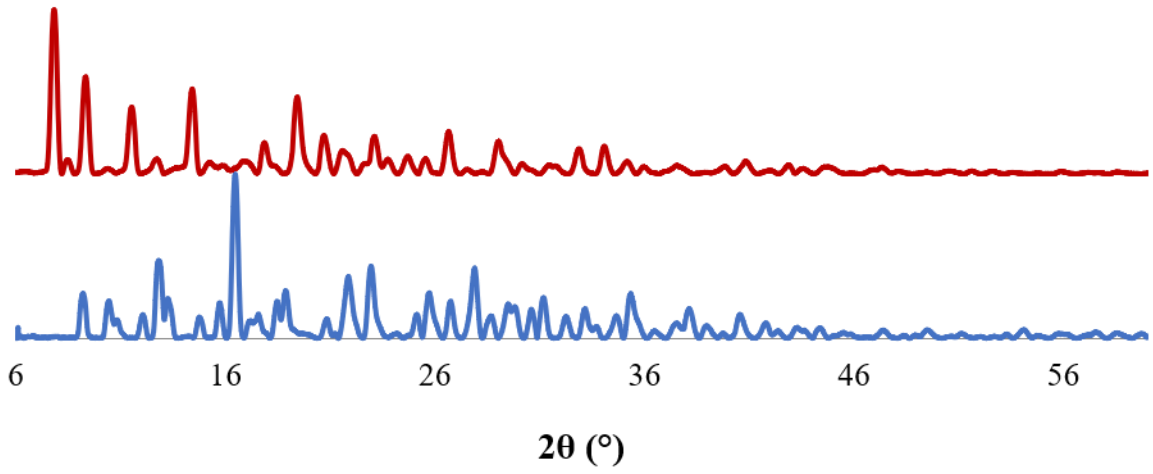

Figure S3.2. Powder X-ray diffractogram overlay of "as received" ZOLE (bottom, blue) and synthetized ZOLE-Ca form II (top, red).

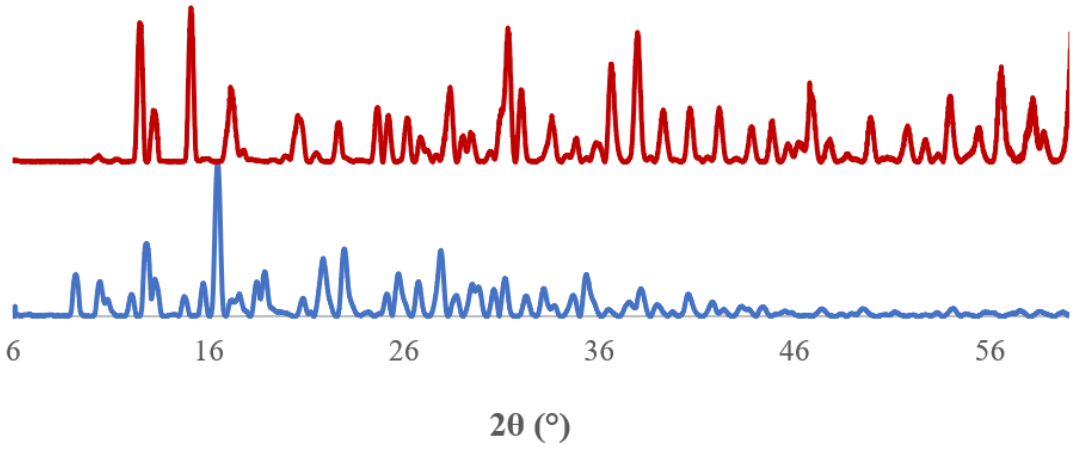

Figure S3.3. Powder X-ray diffractogram overlay of "as received" ZOLE (bottom, blue) and synthetized ZOLE-Mg form I (top, red).

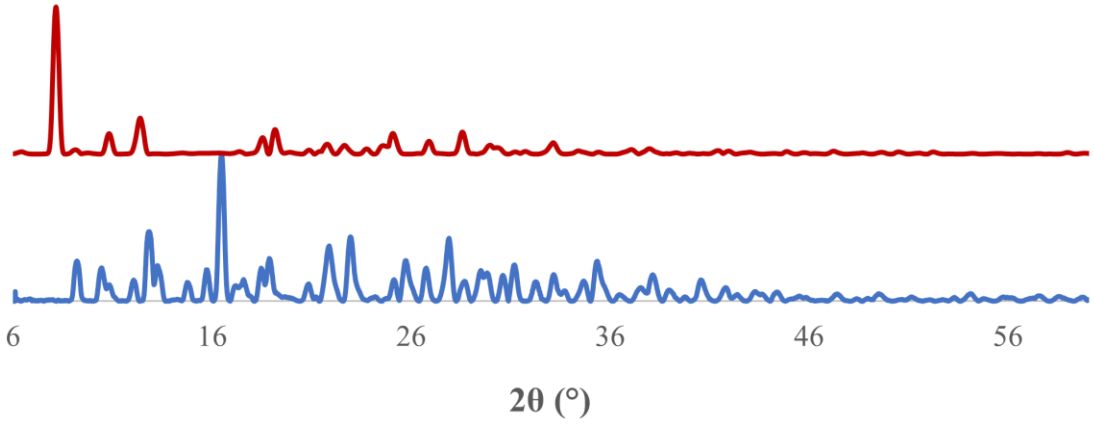

Figure S3.4. Powder X-ray diffractogram overlay of "as received" ZOLE (bottom, blue) and synthetized ZOLE-Mg form II (top, red).

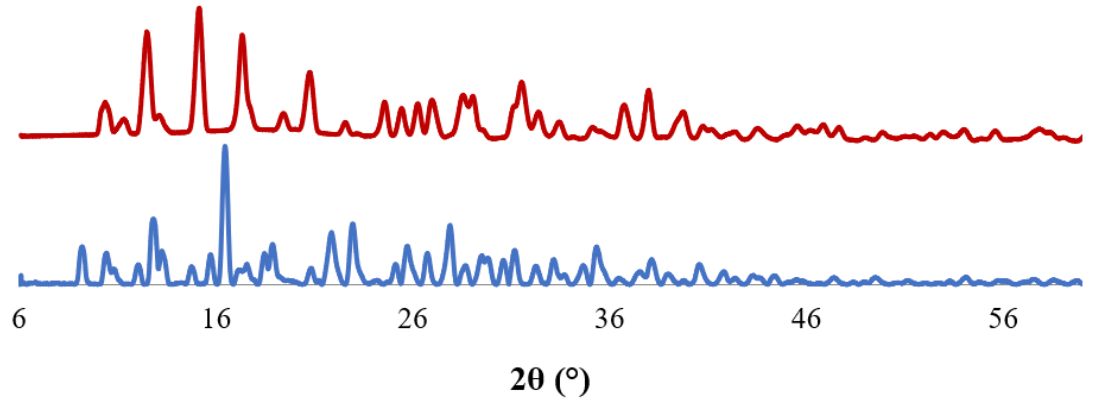

Figure S3.5. Powder X-ray diffractogram overlay of "as received" ZOLE (bottom, blue) and synthetized ZOLE-Zn form I (top, red).

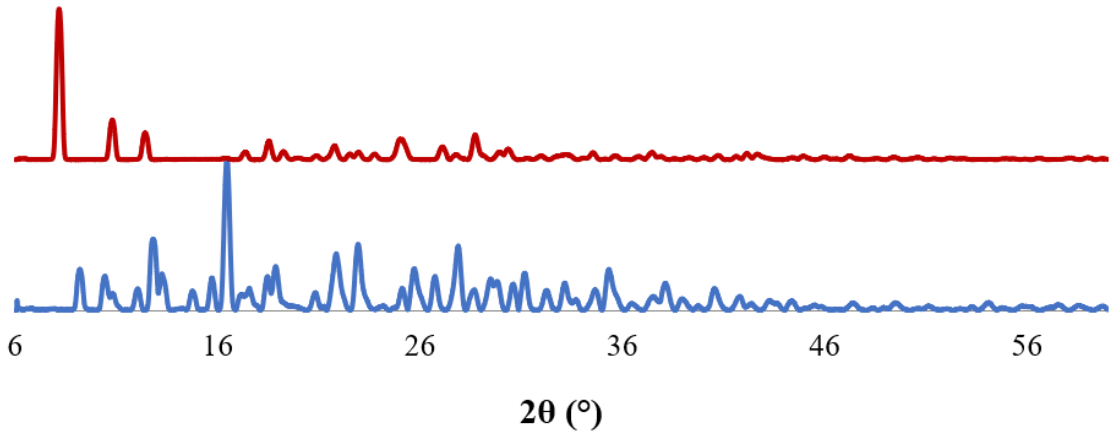

Figure S3.6. Powder X-ray diffractogram overlay of "as received" ZOLE (bottom, blue) and synthetized ZOLE-Zn form II (top, red).

4. Single Crystal X-ray Diffraction (SCXRD)

Figures S4.1-S4.6 display the ball-stick representation of the asymmetric unit and crystalline packing for the refined structures. Figures 4.7-4.12 show the Oak Ridge Thermal Ellipsoid Plots (ORTEPs) for each crystal structure of the ZOLE-based BPCCs. Figures S4.13-S4.18 depict an overlay of the simulated and experimental powder patterns for all structures solved. Figures S4.19-S4.23 show distinct overlays of the simulated powder diffraction pattern overlay for other previously known structures of ZOLE coordination complexes in comparison to the structures solved within this work.[1,2,3,4,5] Simulated PXRDs were extracted from the crystallographic information files (CIF files) obtained from the Cambridge Structural Database or obtained within this work.

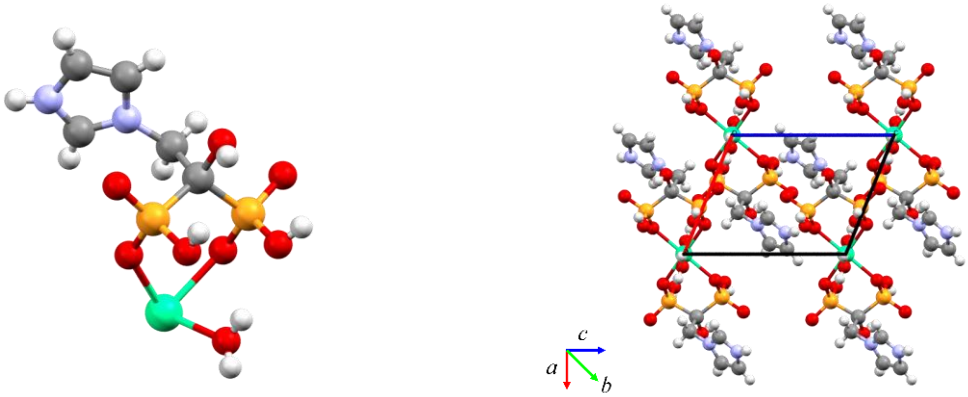

(a) (b)

Figure S4.1. Ball-stick representation of the (a) asymmetric unit and (b) crystalline packing of ZOLE-Ca form I along *b*-axis.

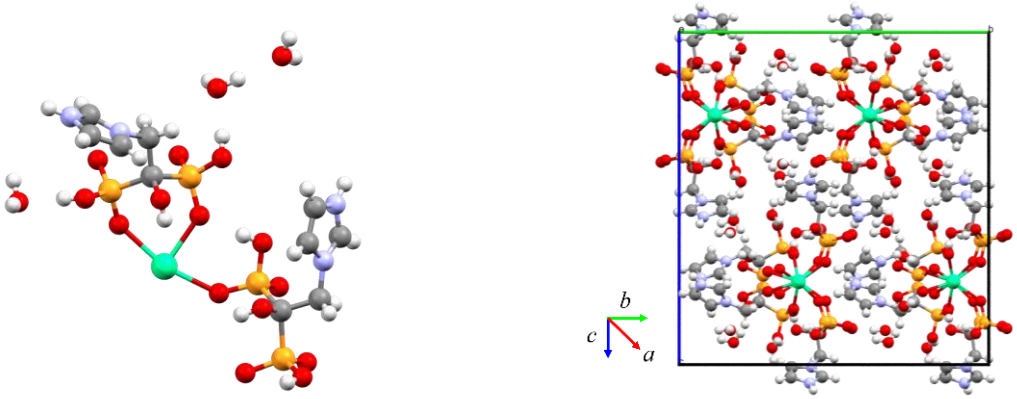

(a) (b)

Figure S4.2. Ball-stick representation of the (a) asymmetric unit and (b) crystalline packing of ZOLE-Ca form II along *a*-axis

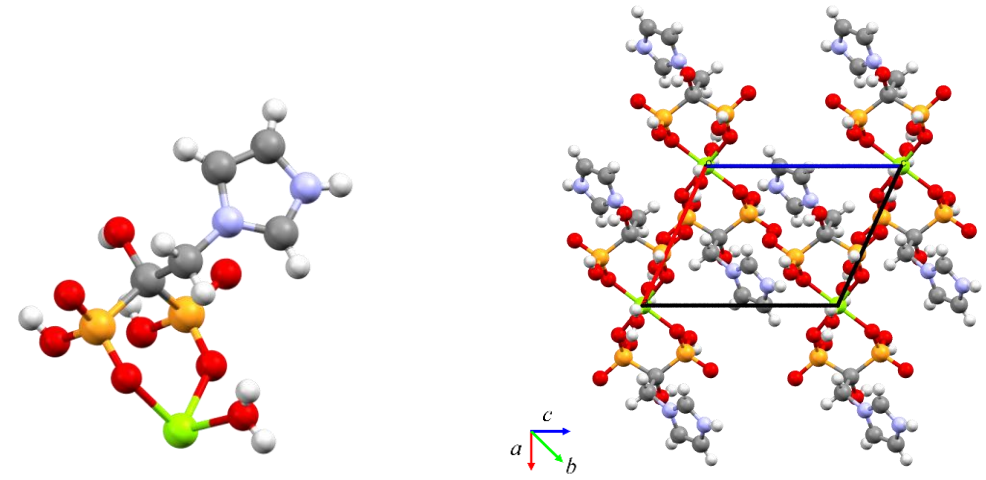

(a) (b)

Figure S4.3. Ball-stick representation of the (a) asymmetric unit and (b) crystalline packing of ZOLE-Mg form I along *b*-axis

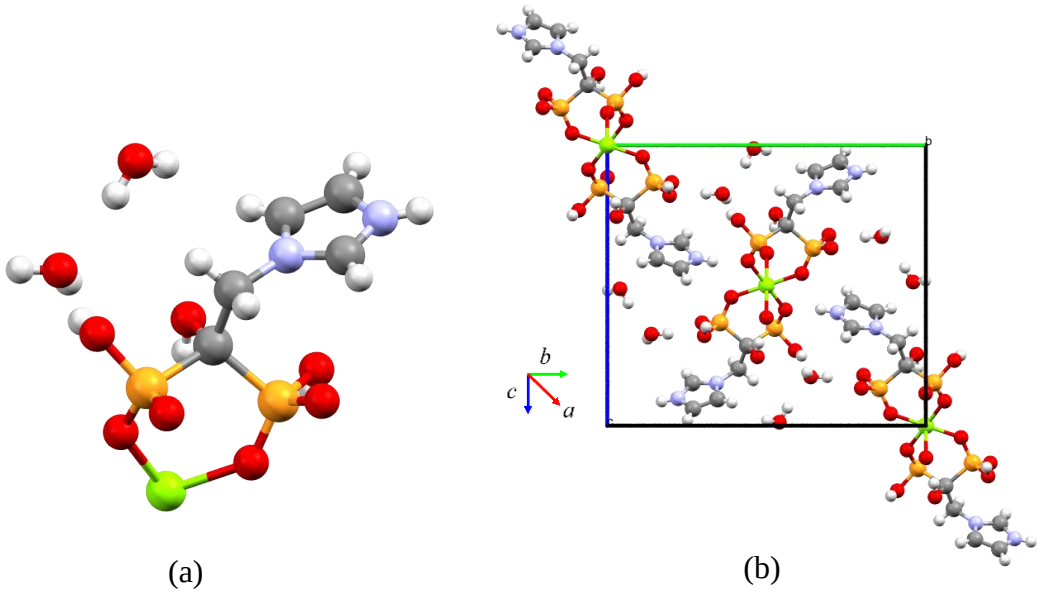

(a) (b)

Figure S4.4. Ball-stick representation of the (a) asymmetric unit and (b) crystalline packing of ZOLE-Mg form II along *a*-axis.

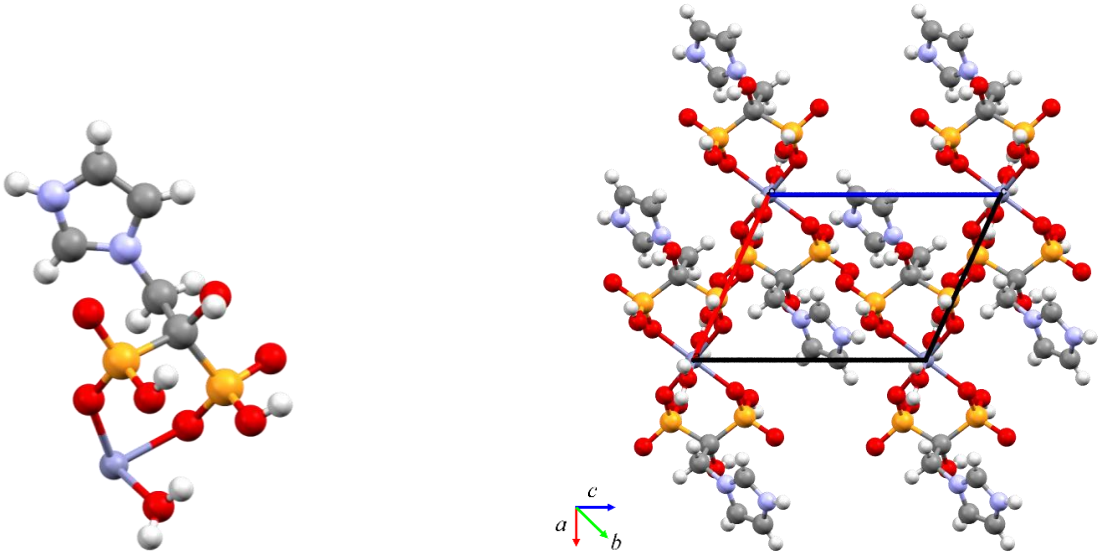

(a) (b)

Figure S4.5. Ball-stick representation of the (a) asymmetric unit and (b) crystalline packing of ZOLE-Zn form I along *b*-axis

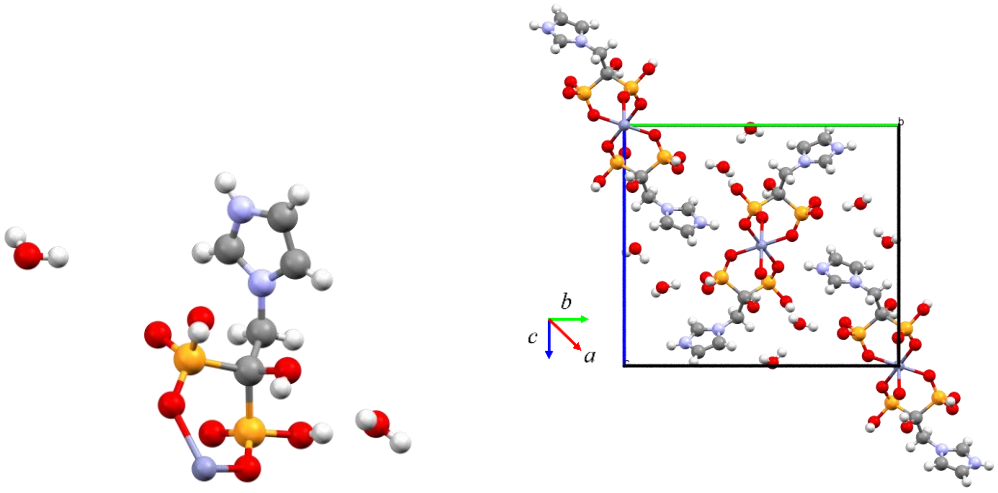

(a) (b)

Figure S4.6. Ball-stick representation of the (a) asymmetric unit and (b) crystalline packing of ZOLE-Zn form II along *a*-axis

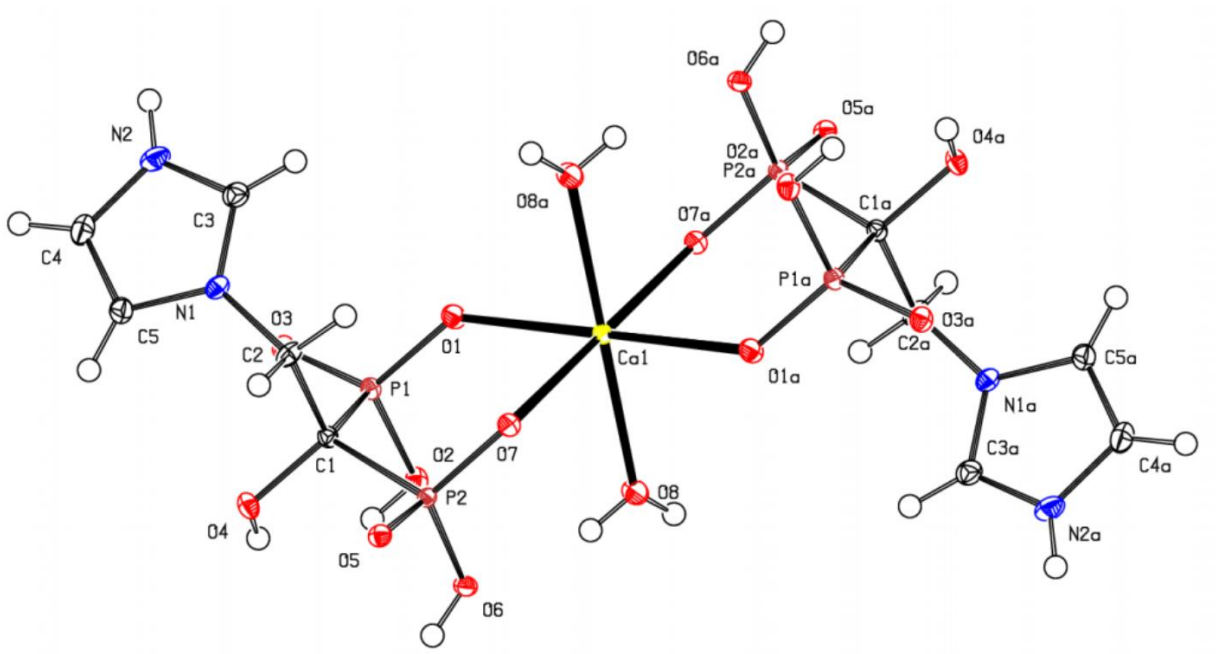

Figure S4.7. ORTEPs (atoms labeled) showing the connectivity between Ca atom and ZOLE to form the ZOLE-Ca form I.

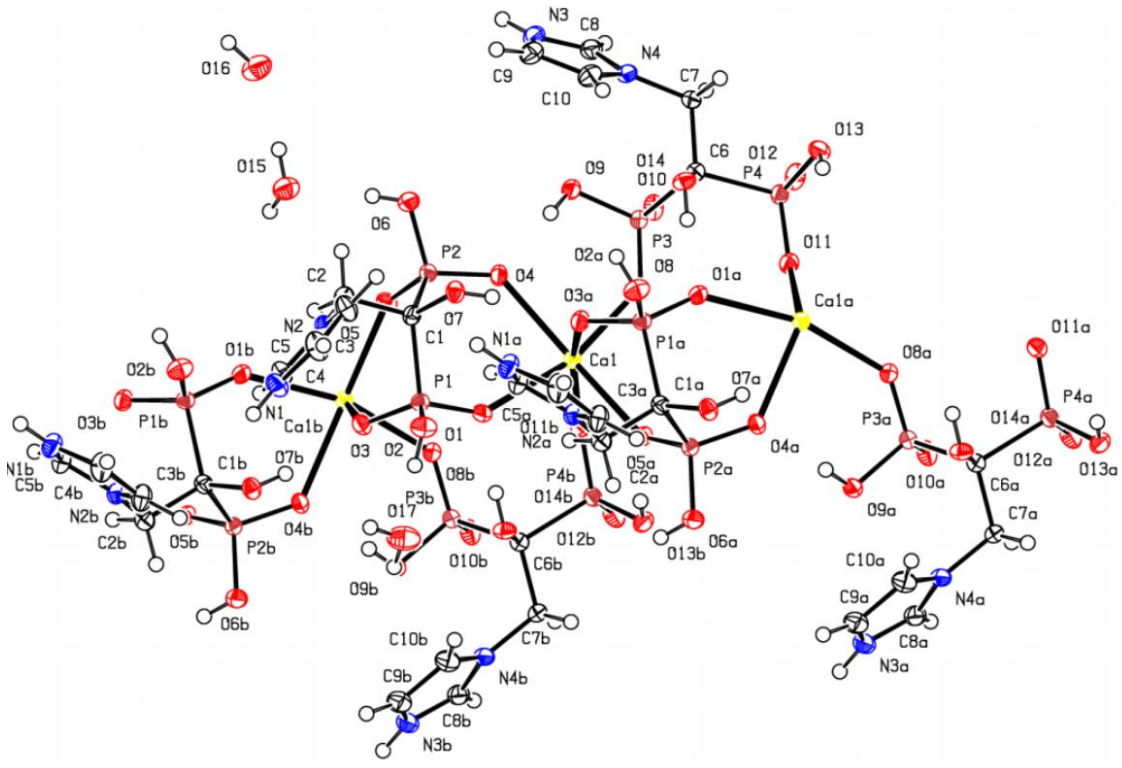

Figure S4.8. ORTEPs (atoms labeled) showing the connectivity between Ca atom and ZOLE to form the ZOLE-Ca form II.

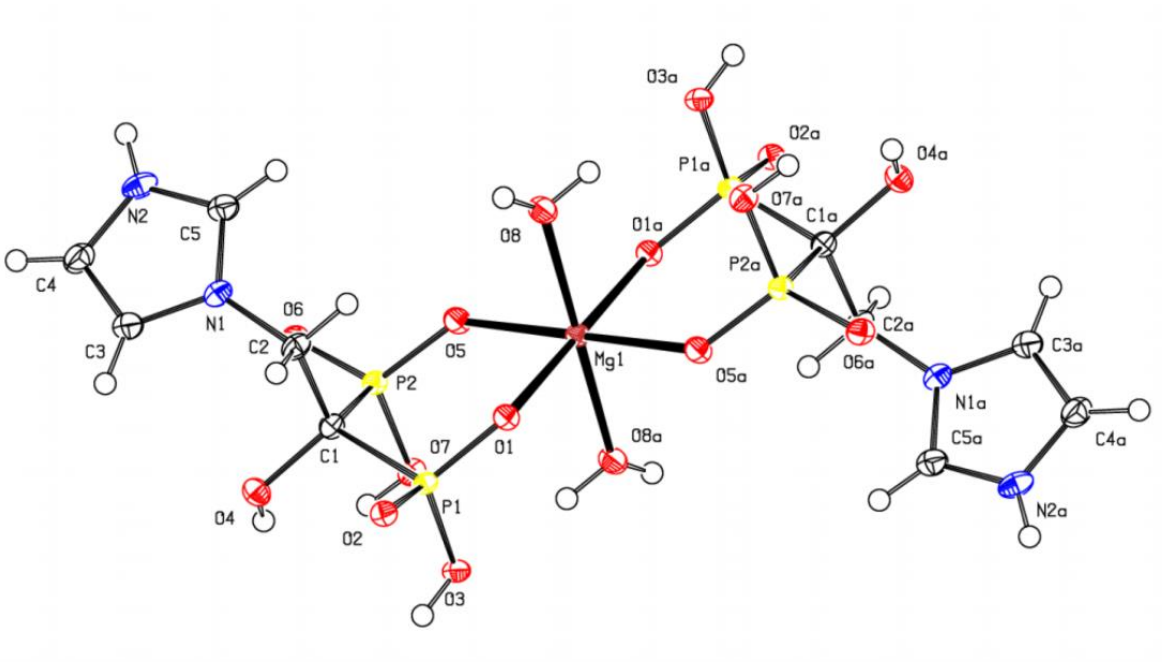

Figure S4.9. ORTEPs (atoms labeled) showing the connectivity between Mg atom and ZOLE to form the ZOLE-Mg form I.

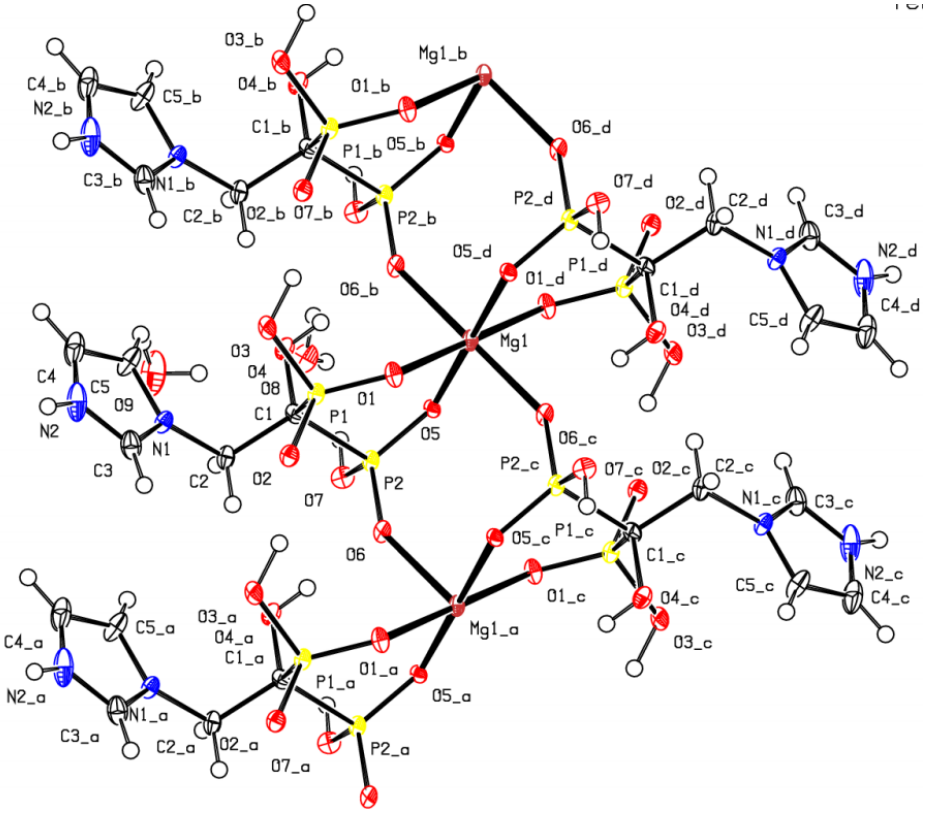

Figure S4.10. ORTEPs (atoms labeled) showing the connectivity between Mg atom and ZOLE to form the ZOLE-Mg form II.

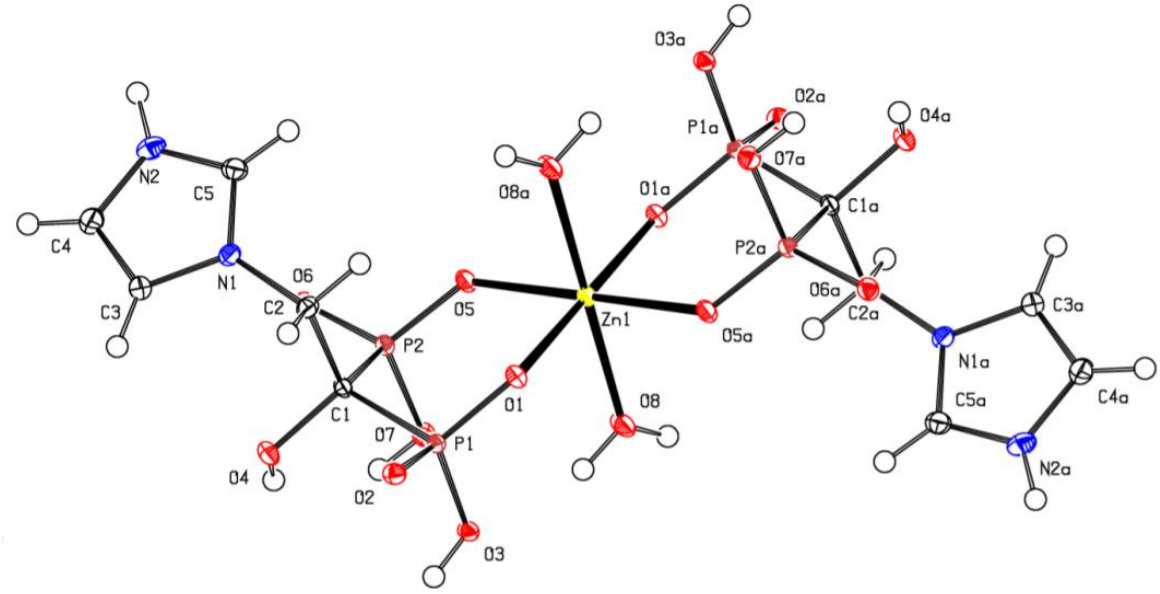

Figure S4.11. ORTEPs (atoms labeled) showing the connectivity between Zn atom and ZOLE to form the ZOLE-Zn form I.

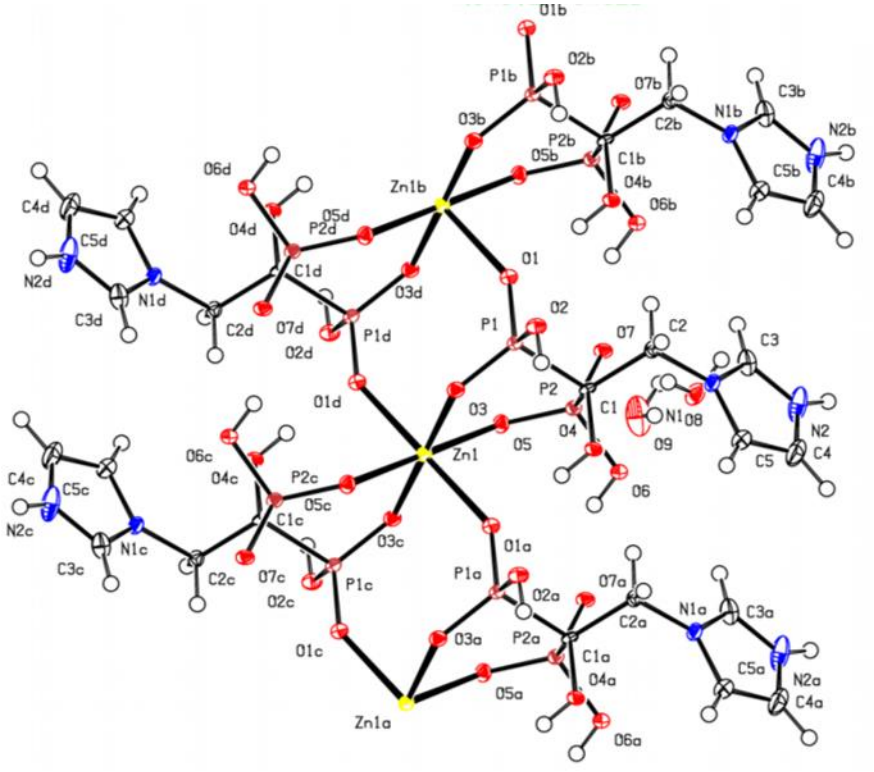

Figure S4.12. ORTEPs (atoms labeled) showing the connectivity between Zn atom and ZOLE to form the ZOLE-Zn form II.

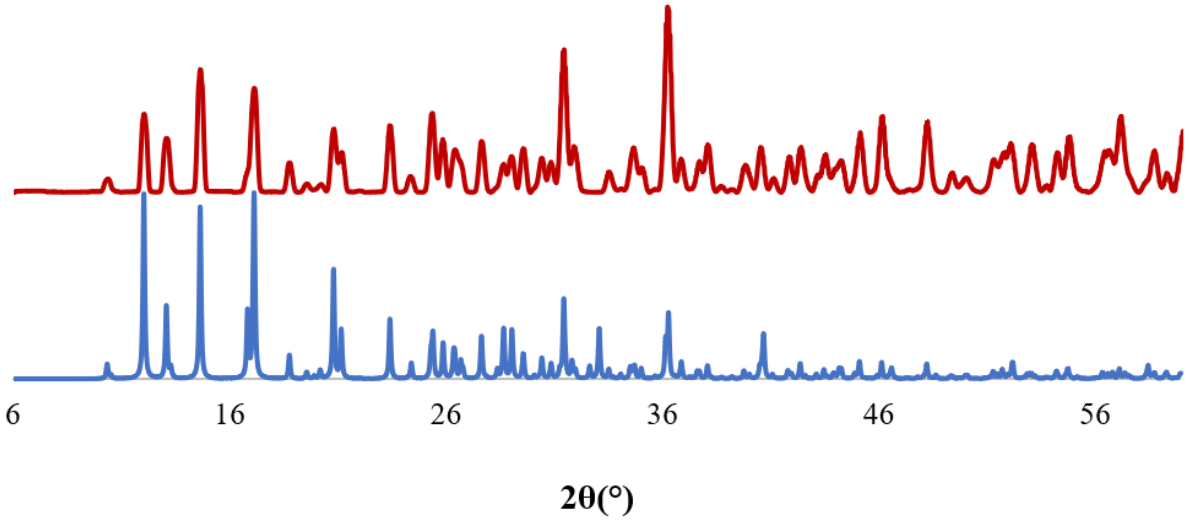

Figure S4.13. Simulated (bottom, blue) and experimental (top, red) powder pattern overlay of ZOLE-Ca form I.

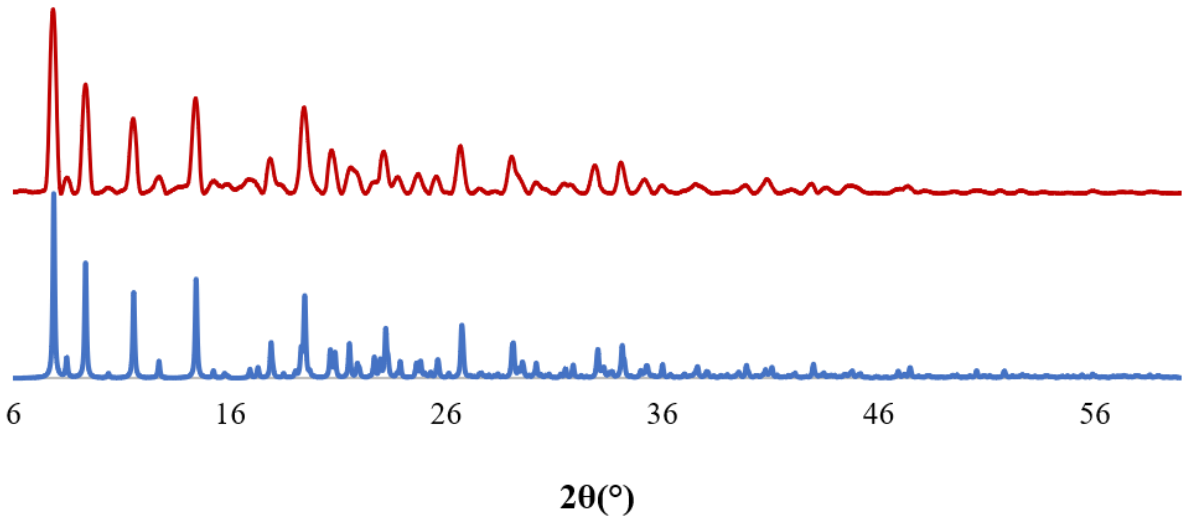

Figure S4.14. Simulated (bottom, blue) and experimental (top, red) powder pattern overlay of ZOLE-Ca form II.

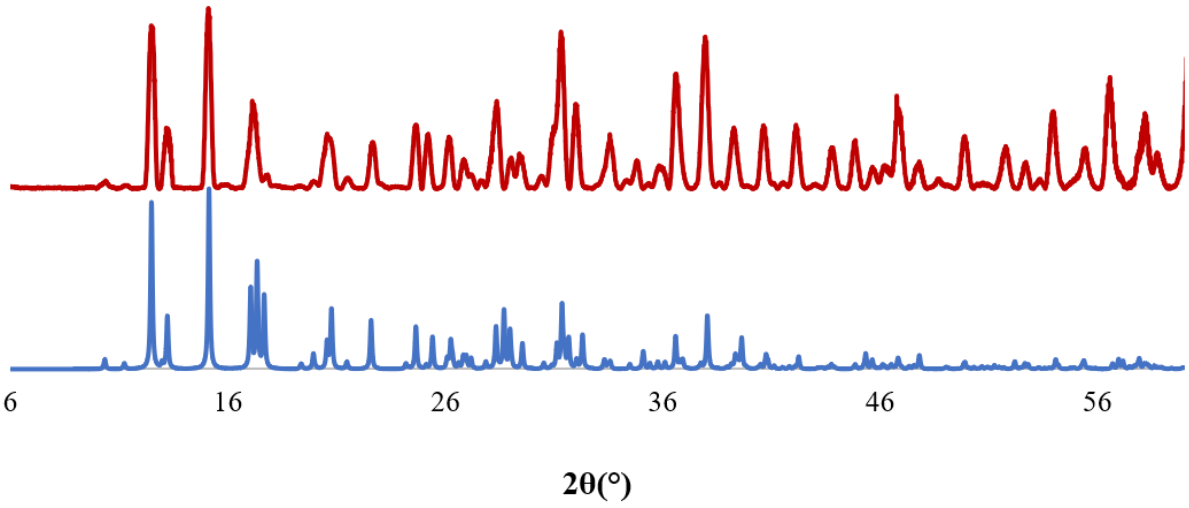

Figure S4.15. Simulated (bottom, blue) and experimental (top, red) powder pattern overlay of ZOLE-Mg form I.

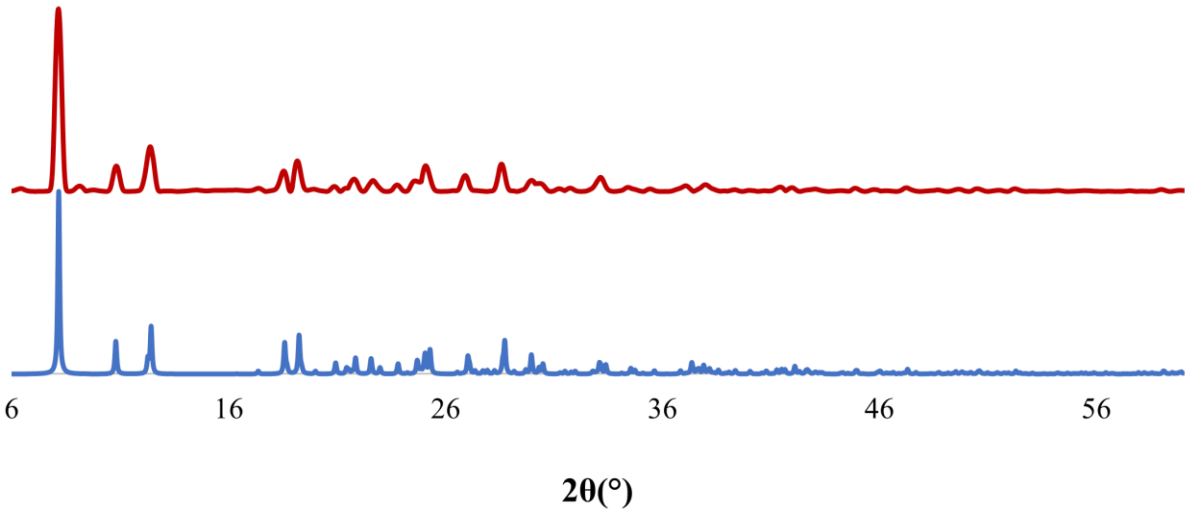

Figure S4.16. Simulated (bottom, blue) and experimental (top, red) powder pattern overlay of ZOLE-Mg form II.

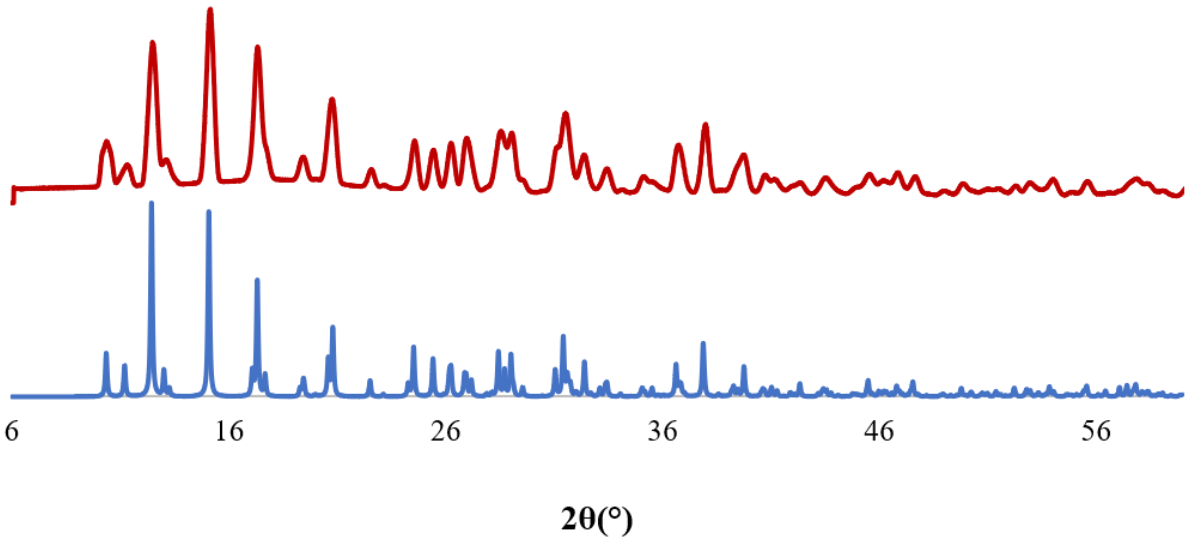

Figure S4.17. Simulated (bottom, blue) and experimental (top, red) powder pattern overlay of ZOLE-Zn form I.

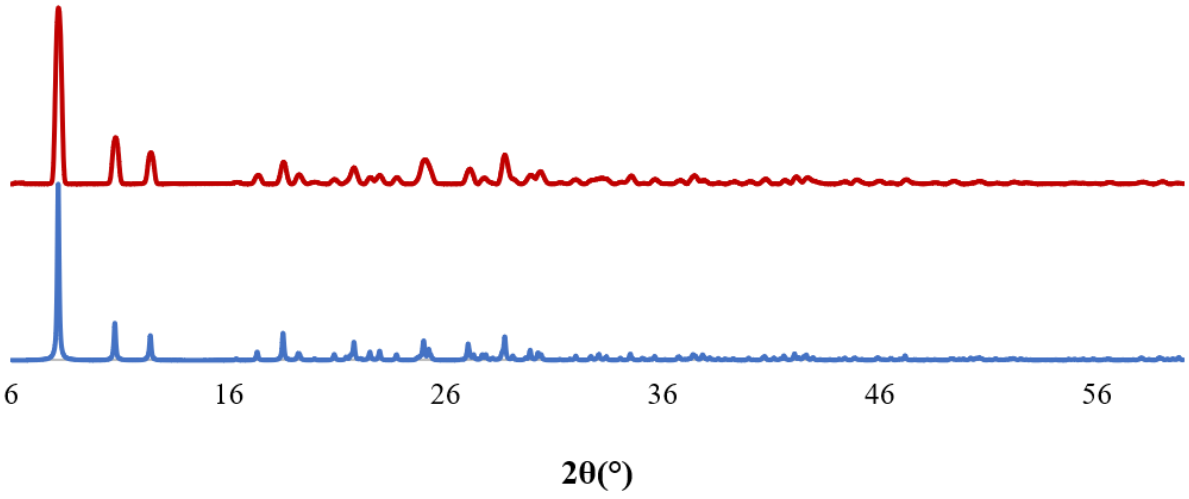

Figure S4.18. Simulated (bottom, blue) and experimental (top, red) powder pattern overlay of ZOLE-Zn form II.

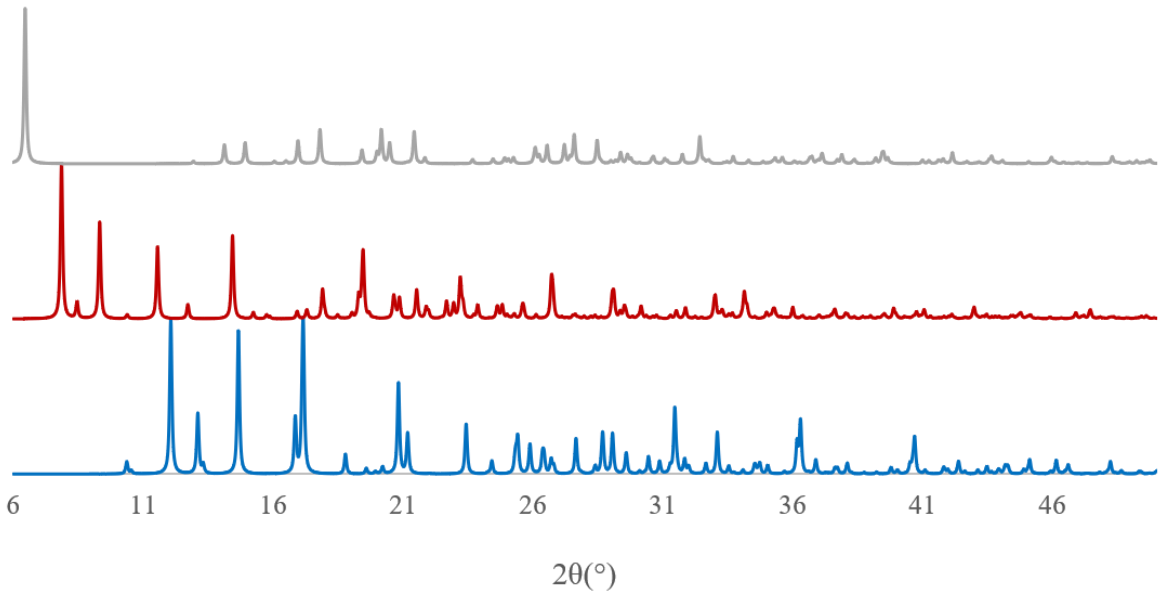

Figure S4.19. Simulated powder pattern overlay of BPCCs containing calcium (Ca^{2+}) from bottom to top; ZOLE-Ca forms I (blue) and II (red) determined within this work and a previously reported metal complex ZOLE-Ca (TUVZEQ[1], light grey).

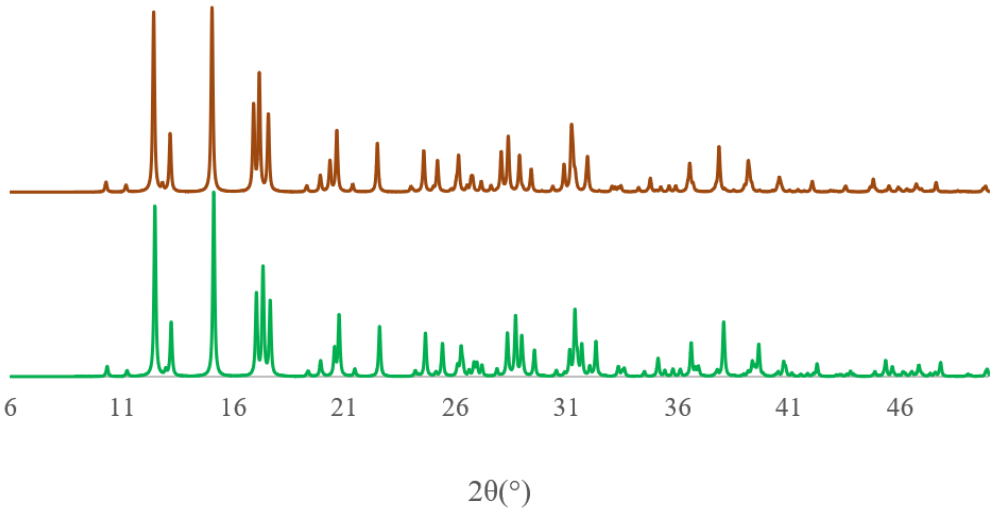

Figure S4.20. Simulated powder pattern overlay of redetermined structure for the synthesized BPCC from bottom to top; ZOLE-Mg form I (green), and the already reported metal complex ZOLE-Mg (TUVZAM, mahogany).[1]

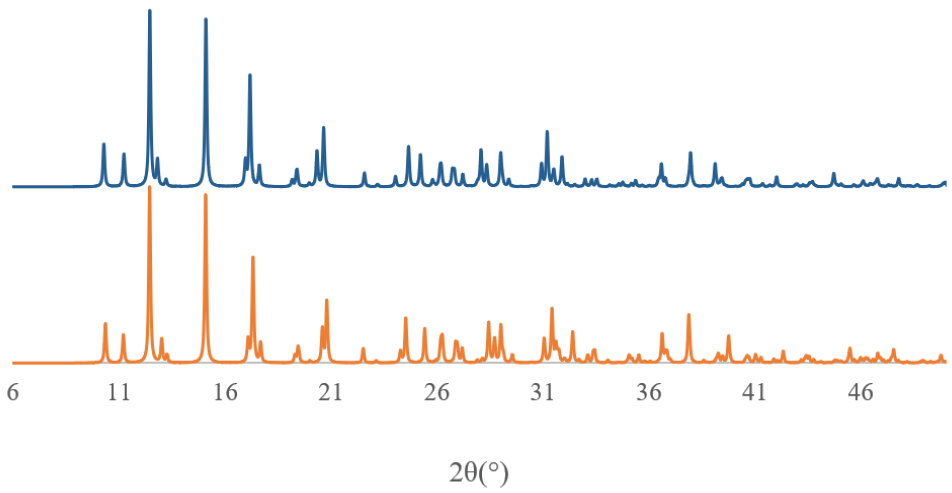

Figure S4.21. Simulated powder pattern overlay of redetermined structure for the synthesized BPCC from bottom to top; ZOLE-Zn form I (green), and the already reported metal complex ZOLE-Zn (PUFXUK, navy blue).[4]

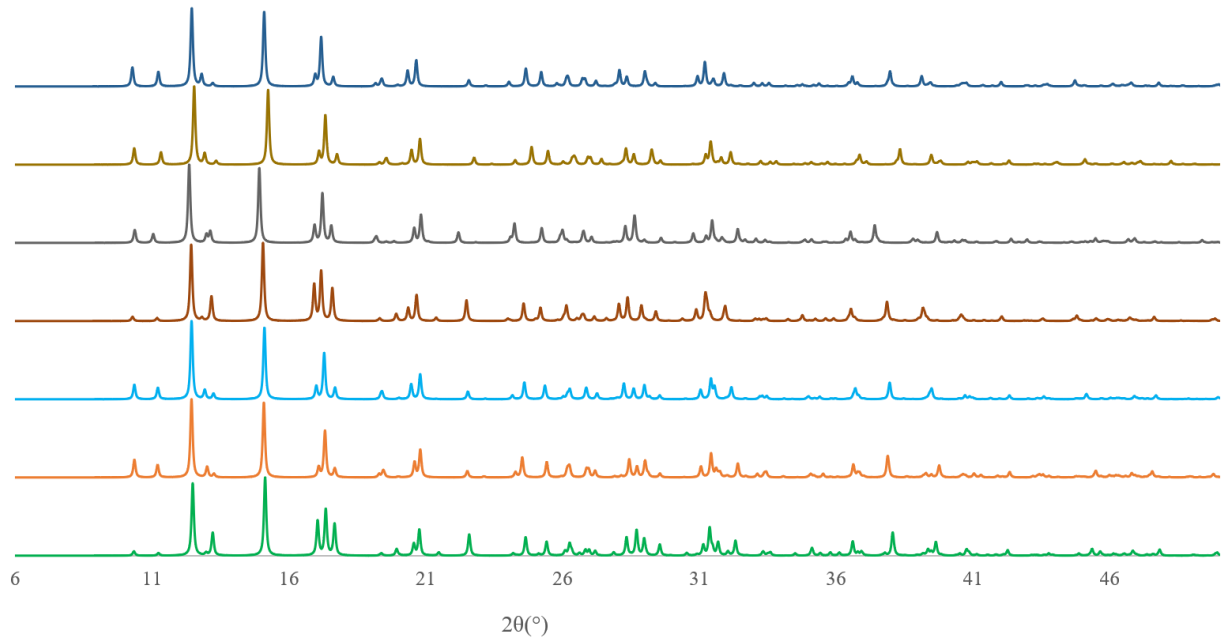

Figure S4.22. Simulated powder pattern overlay of isostructural synthesized BPCCs from bottom to top; ZOLE-Mg form I (green) and ZOLE-Zn form I (orange), and previously reported isostructural forms of ZOLE metal complexes: ZOLE-Co (VIMXOF, light blue),[2] ZOLE-Mg (TUVZAM, mahogany),[1] ZOLE-Mn (RUPXAC, dark grey),[3] ZOLE-Ni (brown, VIMXUL),[2] and ZOLE-Zn (PUFXUK, navy blue).[4]

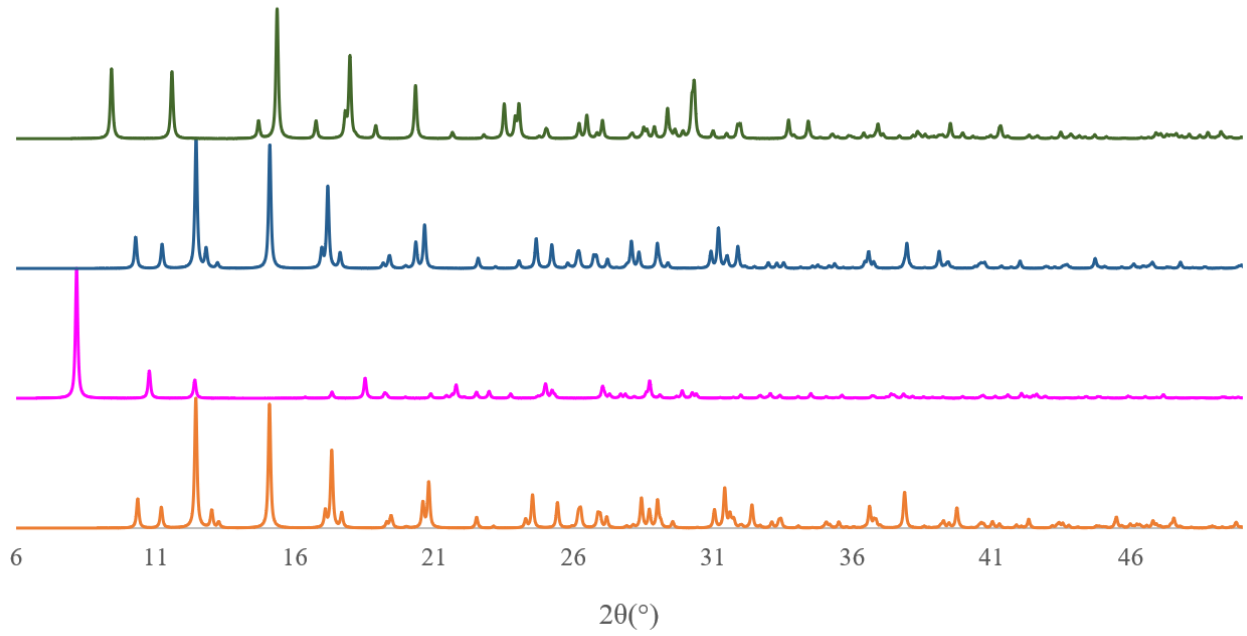

Figure S4.23. Simulated powder pattern overlay of BPCCs containing zinc (Zn^{2+}) from bottom to top; ZOLE-Zn forms I (orange) and II (pink), and previously reported structures of ZOLE-Zn metal complexes: PUFXUK[4] (navy blue) and PUFYAR[5] (dark green). ZOLE-Zn form I constitutes a redetermination of PUFXUK[4] (navy blue). PUFYAR[5] (dark green) presents a unique packing when compared to all other ZOLE-Zn metal complexes and those described within this work.

5. Thermogravimetric Analysis (TGA)

Figures S5.1-5.5 depict overlay of thermographs for the ZOLE-based BPCCs and ZOLE recorded in a TGA Q500 (TA Instruments Inc.) using a temperature range of 10 – 700°C at 5°C/min under a N_2 gas purge (60 mL/min). In all cases, ~10 mg of powder sample were thermally treated. TGA data was analyzed with TA Universal Analysis software version 4.3A.

For the thermal decomposition of the "as received" ZOLE, a low temperature (50-100 °C) weight loss (6.995 wt. %) was observed, which corresponds to the dehydration of the ligand (trihydrate). Subsequently, at higher temperature (200-700 °C) a weight loss of 67.71 wt. % was observed, which corresponds to the thermal degradation of ZOLE.

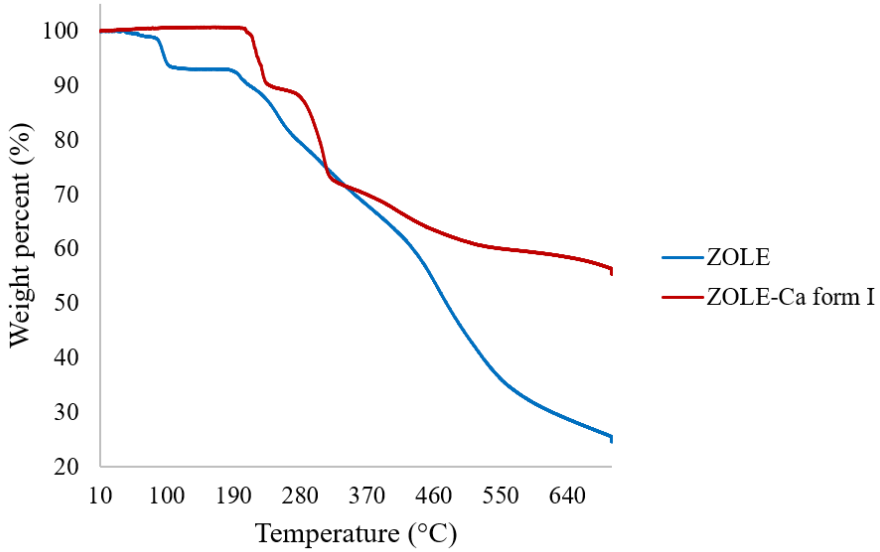

Figure S5.1. TGA analysis of ZOLE-Ca form I BPCC shows an initial thermal degradation event (*exp:* 5.856 wt. %), attributed to the loss of water molecules from the complex (*theo:* 5.83 wt. %). Additionally, TGA analysis shows a low temperature (200-300°C) weight lost (28.00 wt. %), which was attributed to the decomposition of ZOLE. Subsequently at higher temperature (300-700°C) a weight loss of 14.93 wt. % occurred, which was attributed to the degradation of calcium/calcium oxide.

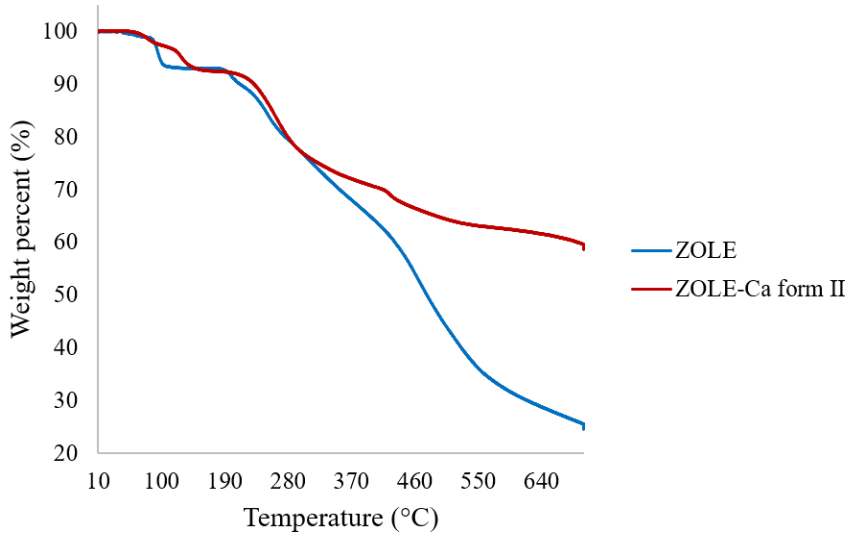

Figure S5.2. TGA analysis of ZOLE-Ca form II BPCC shows a low temperature (50-150°C) weight lost (*exp:* 8.240 wt. %), which was attributed to the evaporation of water molecules (*theo:* 8.50 wt. %). Additionally, another low temperature (200-400°C) weight lost (22.16 wt. %) was observed, which was attributed to the decomposition of ZOLE. Subsequently at higher temperature (400-700°C) a weight loss of 9.936 wt. % occurred, which was attributed to the degradation of calcium/calcium oxide.

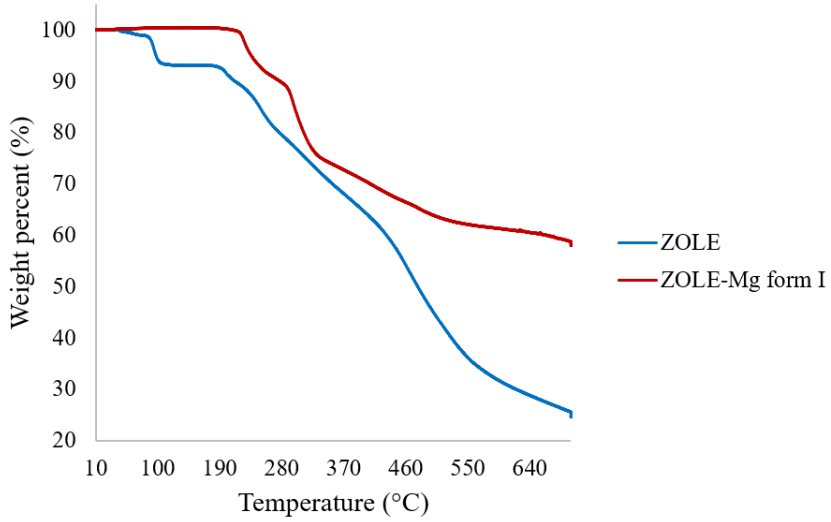

Figure S5.3. TGA analysis of ZOLE-Mg form I BPCC shows an initial thermal degradation event (*exp:* 11.38 wt. %), attributed to the loss of water molecules from the complex (*theo:* 11.96 wt. %). Additionally, TGA analysis shows a low temperature (250-350°C) weight lost (14.88 wt. %), which was attributed to the decomposition of ZOLE. Subsequently at higher temperature (400-700°C) a weight lost (15.60 wt. %) occurred, which was attributed to the degradation of magnesium/magnesium oxide.

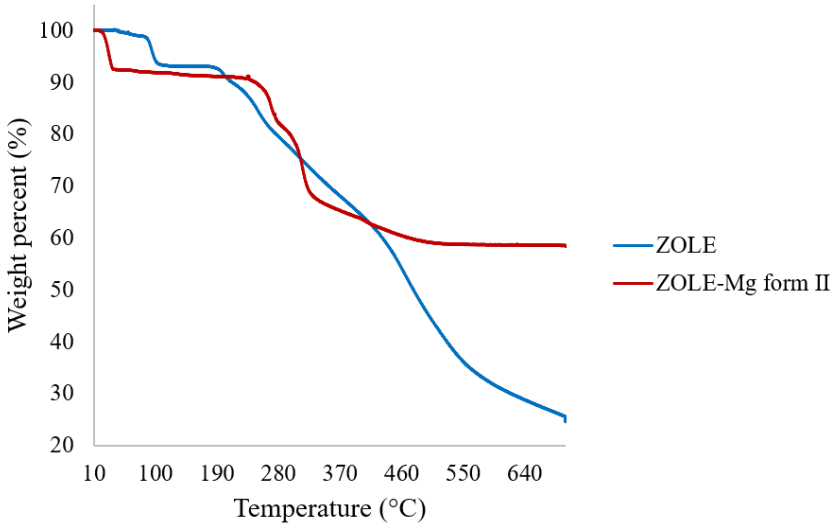

Figure S5.4. TGA analysis of ZOLE-Mg form II BPCC shows an initial thermal degradation event (*exp:* 10.78 wt. %), attributed to the water loss from the complex (*theo:* 11.28 wt. %). Additionally, analysis revealed a low temperature (250-350°C) weight lost (23.14 wt. %), which was attributed to the decomposition of ZOLE. Subsequently at higher temperature (350-700°C) a weight lost (8.930 wt. %) occurred, which was attributed to the degradation of magnesium/magnesium oxide.

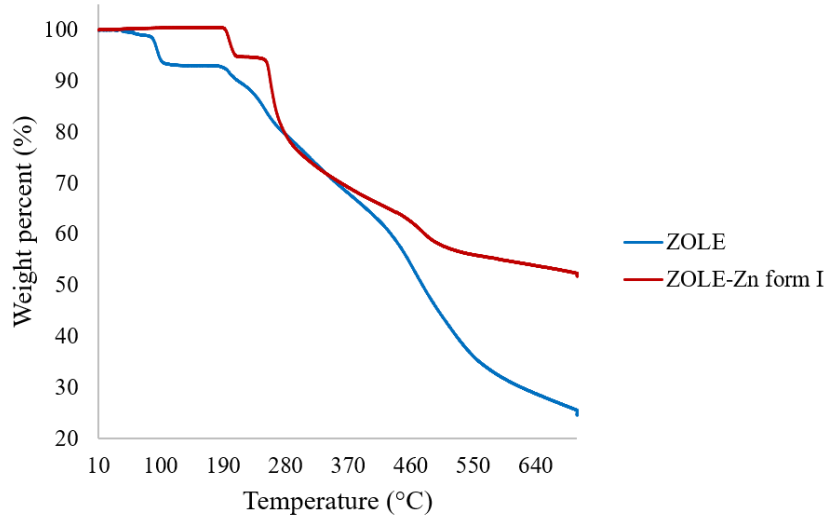

Figure S5.5. TGA analysis of ZOLE-Zn form I BPCC shows a low temperature (190-200°C) weight lost (*exp:* 5.356 wt. %), which was attributed to the evaporation of water molecules (*theo:* 5.60 wt. %). Another low temperature (250-450°C) weight lost (31.37 wt. %), which was attributed to the decomposition of ZOLE was observed. Subsequently, at higher temperature (400-700°C) a weight loss of 10.87 wt. % occurred, which was attributed to the degradation of zinc/zinc oxide.

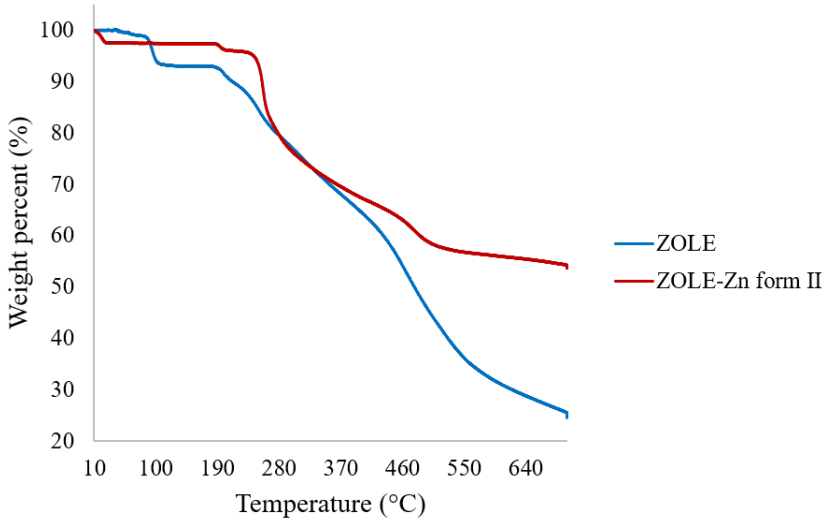

Figure S5.6. TGA analysis of ZOLE-Zn form II BPCC shows a low temperature (10-250°C) weight lost (*exp:* 5.054 wt. %), which was attributed to the evaporation of water molecules (*theo:* 5.30 wt. %). Another low temperature (250-450°C) weight lost (29.63 wt. %) was observed, which was attributed to the decomposition of ZOLE. Subsequently, at higher temperature (450-700°C) a weight loss of 8.375 wt. % occurred, which was attributed to the degradation of zinc/zinc oxide.

6. Scanning Electron Microscopy coupled with Energy Dispersive Spectroscopy

Figures S6.1.1 represent scanning electron micrographs of the ZOLE-based BPCCs showing clusters and single crystals. Figures S6.2.1-S6.2.5 depict the energy dispersive spectra for the synthesized ZOLE-based BPCCs.

6.1. Scanning Electron Micrographs

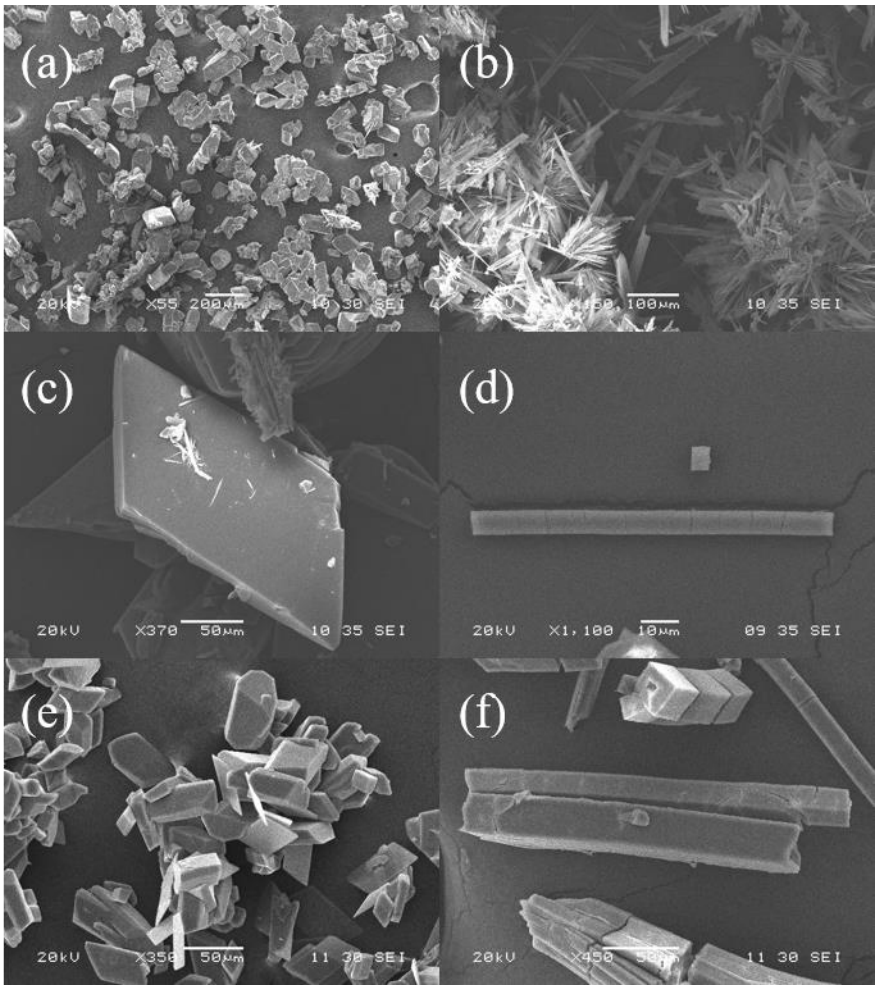

Figure 6.1.1. Scanning electron micrographs for the ZOLE-based BPCCs crystals and clusters; (a) ZOLE-Ca form I, (b) ZOLE-Ca form II, (c) ZOLE-Mg form I, (d) ZOLE-Mg form II, (e) ZOLE-Zn form I, and (f) ZOLE-Zn form II.

6.2. Energy Dispersive Spectra

ZOLE-Ca form I

Figure S6.2.1. Energy dispersive spectra of ZOLE-Ca form I BPCC displaying the presence of atoms (carbon, nitrogen, oxygen and phosphorous) present in ZOLE and the metal (calcium).

ZOLE-Ca form II

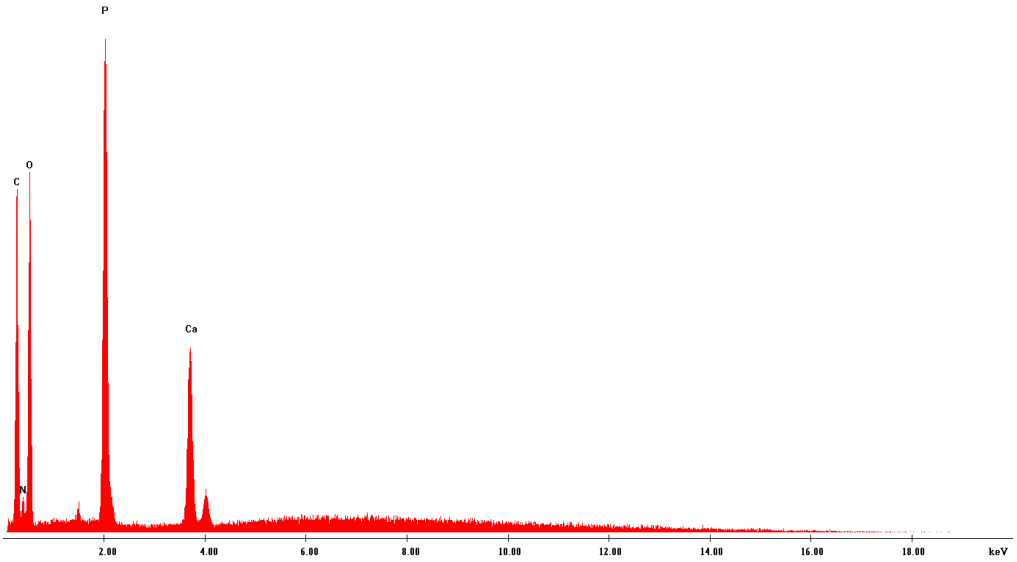

Figure S6.2.2. Energy dispersive spectra of ZOLE-Ca form II BPCC displaying the presence of atoms (carbon, nitrogen, oxygen and phosphorous) present in the ligand and the metal (calcium).

ZOLE-Mg form I

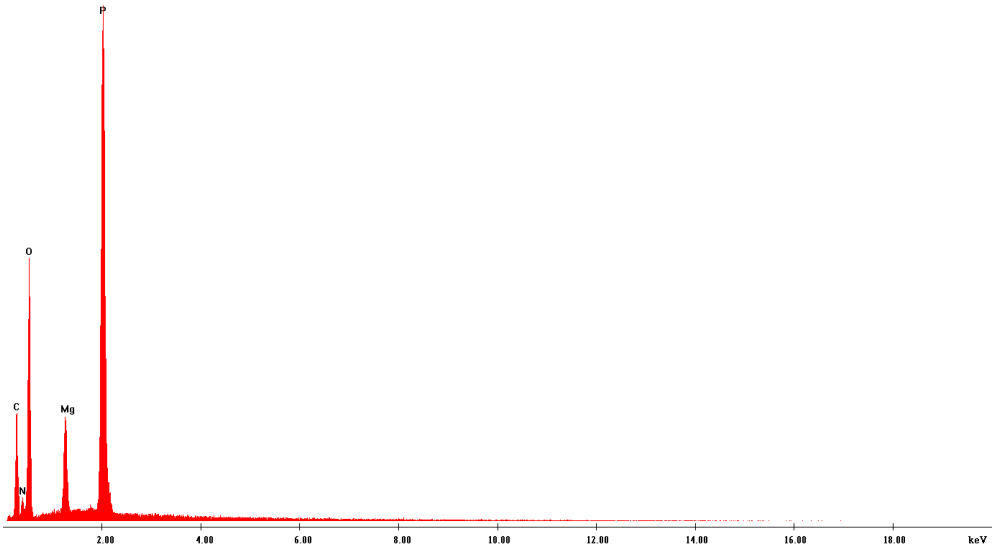

Figure S6.2.3. Energy dispersive spectra of ZOLE-Mg form I BPCC displaying the presence of atoms (carbon, nitrogen, oxygen and phosphorous) present in the ligand and the metal (magnesium).

ZOLE-Mg form II

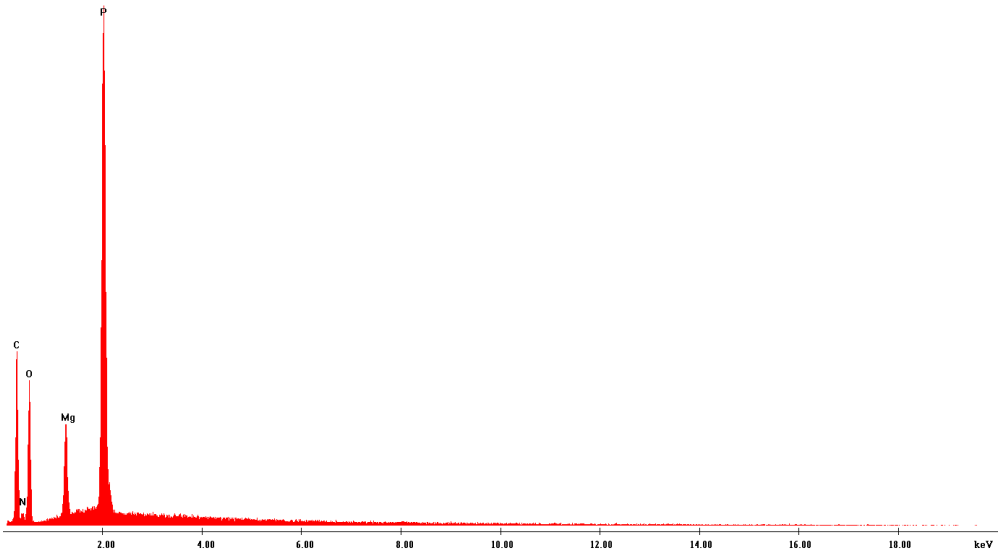

Figure S6.2.4. Energy dispersive spectra of ZOLE-Mg form II BPCC displaying the presence of atoms (carbon, nitrogen, oxygen and phosphorous) present in the ligand and the metal (magnesium).

ZOLE-Zn form I

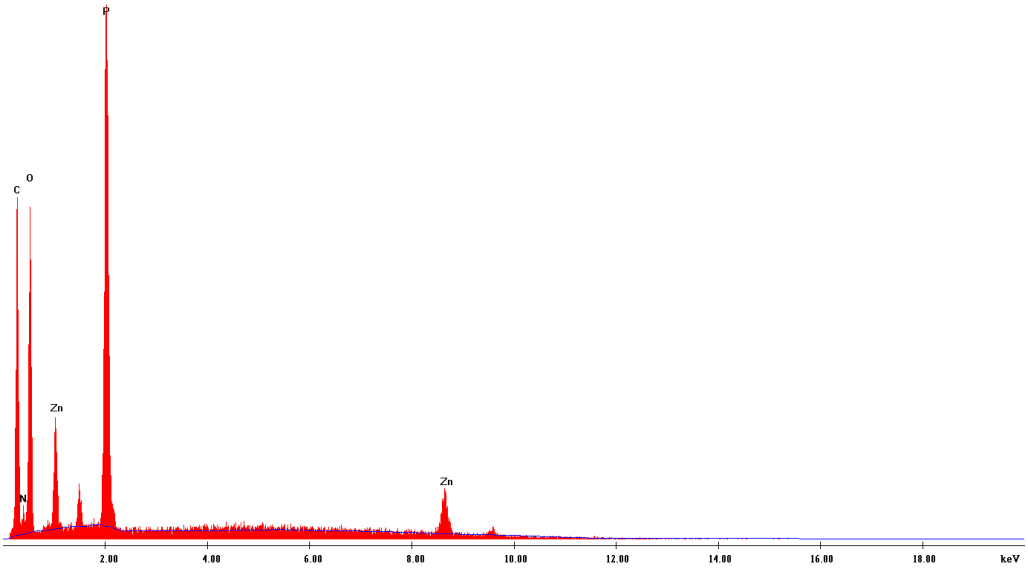

Figure S6.2.5. Energy dispersive spectra of ZOLE-Zn form I BPCC displaying the presence of atoms (carbon, nitrogen, oxygen and phosphorous) present in the ligand and the metal (zinc).

ZOLE-Zn form II

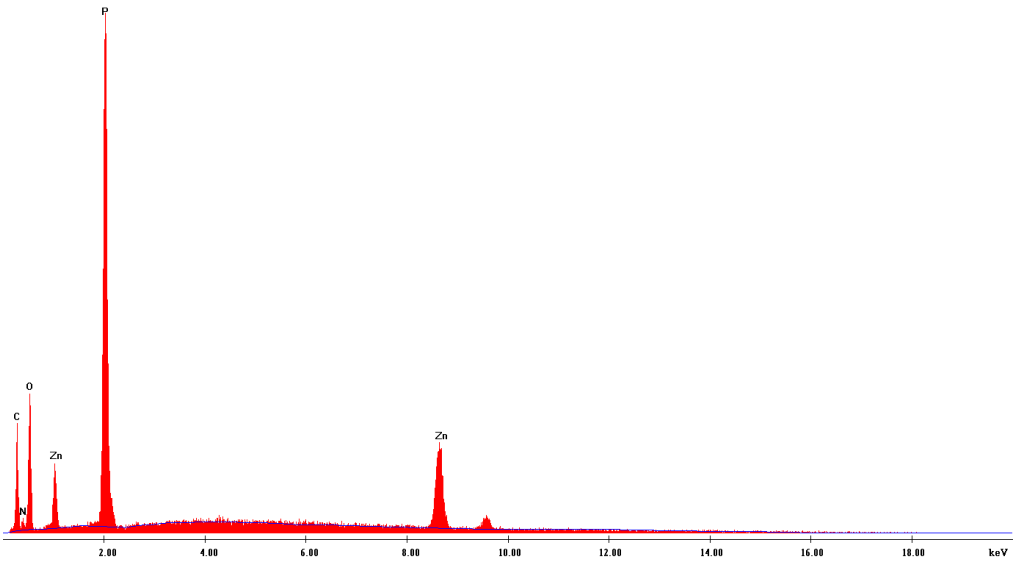

Figure S6.2.6. Energy dispersive spectra of ZOLE-Zn form II BPCC displaying the presence of atoms (carbon, nitrogen, oxygen and phosphorous) present in the ligand and the metal (zinc).

7. Dissolution Profiles for ZOLE-based BPCCs

Dissolution Profiles in PBS

Stock Solution: Standard stock solution of ZOLE was prepared by dissolving 25 mg of the drug in a 100 mL volumetric flask using PBS as media. More dilute solutions were obtained by appropriate dilution from this stock solution (see *Calibration Curve* section).

Calibration Curve: Accurately measured aliquots of the ZOLE stock solution were transferred into a series of 25 mL volumetric flasks to achieve a concentration range between 0.001-0.06 mg/mL. Each solution was completed to the 25 mL mark with PBS.

Dissolution Profile: Dissolution profiles were recorded for ZOLE, ZOLE-Ca forms I and II, ZOLE-Mg forms I and II, and ZOLE-Zn forms I and II. Dissolution tests were performed in 100 mL of PBS buffer (pH = 7.40), controlling temperature at 37°C and stirring at 150 rpm. For the ZOLE-based BPCCs and ZOLE, 25 mg of the solid were grinded using a mortar and pestle. The powder was added to the PBS solution at the beginning of the dissolution under stirring. Samples of 1.0 mL were collected after 0, 0.0083, 0.017, 0.083, 0.17, 0.5, 1, 3, 6, 18, 24 and 48 h to record the complete dissolution profile. For ZOLE-Zn form I, sample collection was extended for 72, 144, 168 and 192 h to reach the equilibrium solubility. The samples were placed in 5 mL volumetric flasks and completed to volume with PBS. The absorbance was measured at λ_{max} = 208 nm against a reagent blank in a 400-200 nm scan range using an Agilent Technologies Cary Series UV-Vis spectrophotometer, Cary 100 UV-Vis mode and the UV Cary Scan software (version v.20.0.470).

Figures S7.1-S7.2 depict the absorption spectra with the respective calibration curve for the ZOLE quantification in PBS. Figure S7.3 shows the extended dissolution profile for ZOLE-Zn form I BPCC (192 h).

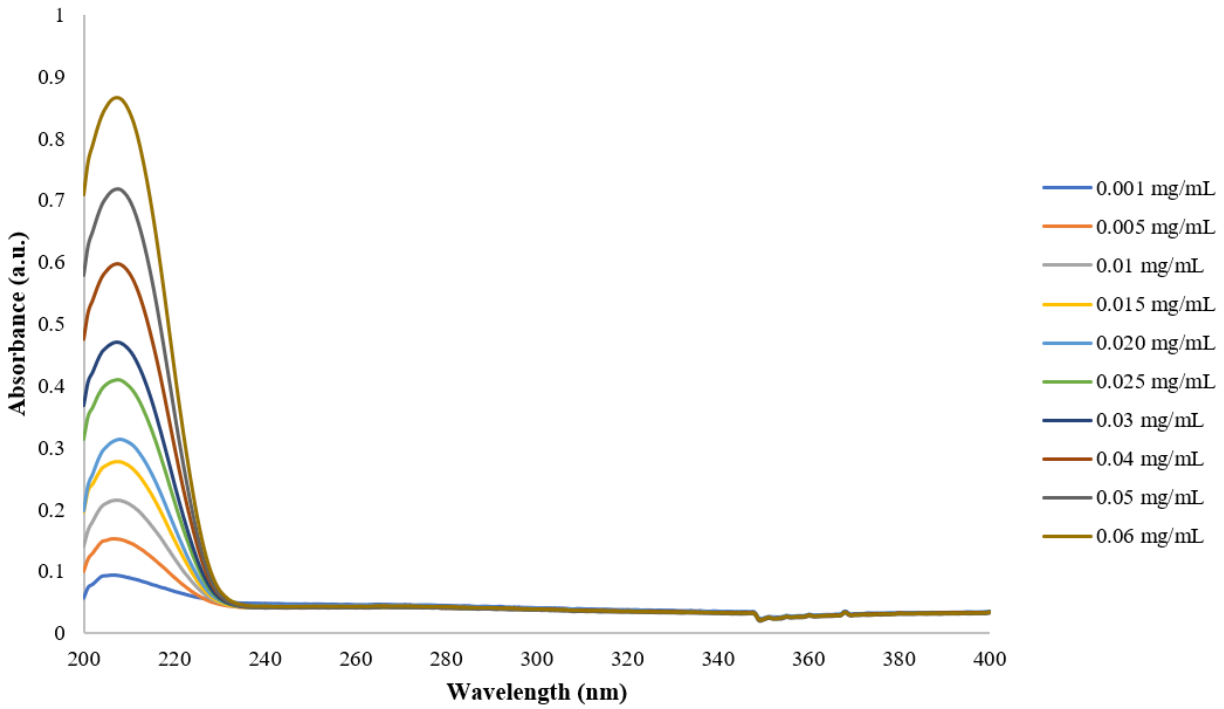

Figure S7.1. Absorbance spectra of ZOLE presenting a λ_{max} at 208 nm in PBS in the concentration range of 0.001-0.06 mg/mL employed to construct a calibration curve.

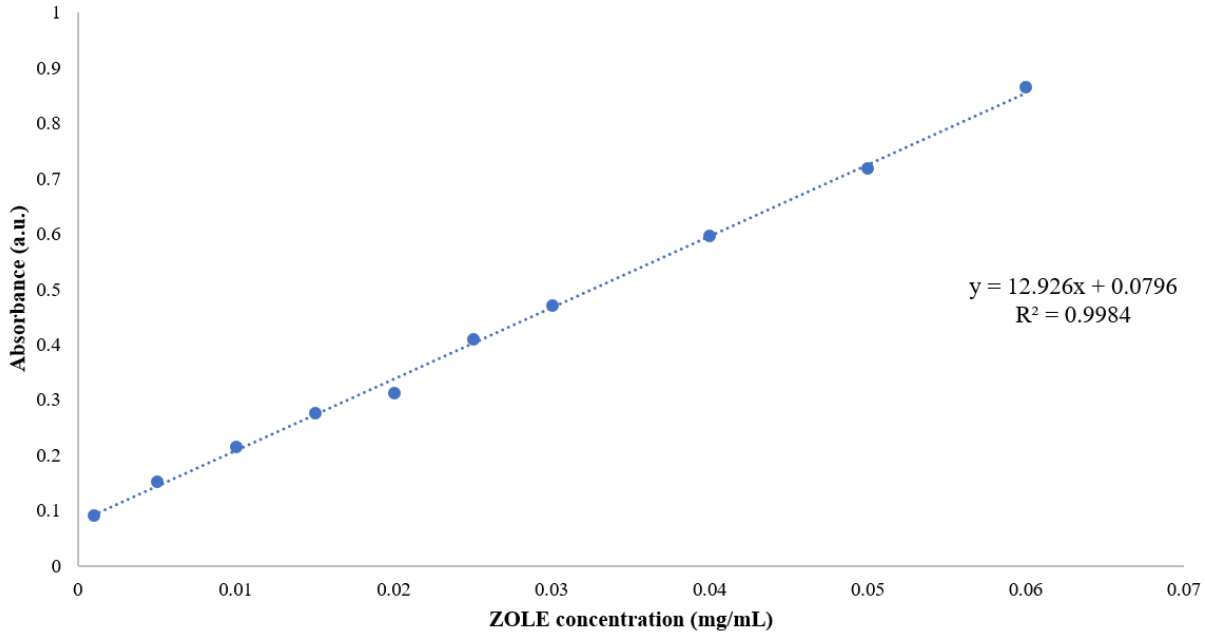

Figure S7.2. Calibration curve for ZOLE quantification for ZOLE-based BPCCs in PBS.

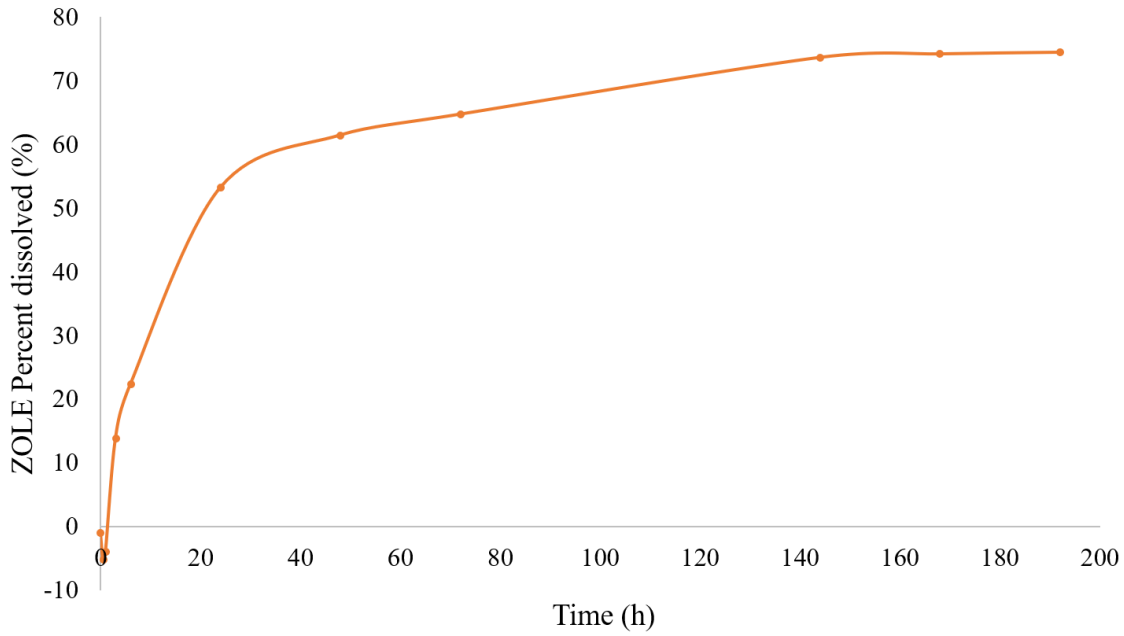

Figure S7.3. Extended dissolution profile (192 h) in PBS for ZOLE-Zn form I (orange), reaching a plateau regarding its equilibrium solubility at 144 h.

Dissolution Profiles in FaSSGF

Stock Solution: Standard stock solution of ZOLE was prepared by dissolving 25 mg of the drug in a 100 mL volumetric flask using FaSSGF as media. More dilute solutions were obtained by appropriate dilution from this stock solution (see *Calibration Curve* section).

Calibration Curve: Accurately measured aliquots of the ZOLE stock solution were transferred into a series of 25 mL volumetric flasks to achieve a concentration range between 0.001-0.06 mg/mL. Each solution was completed to the 25 mL mark with FaSSGF.

Dissolution Profile: Dissolution profiles were recorded for ZOLE and ZOLE-Ca form II. Dissolution tests were performed in 100 mL of FaSSGF buffer (pH = 1.60), controlling temperature at 37°C and stirring at 150 rpm. For the ZOLE-based BPCC and ZOLE, 25 mg of the solid were grinded using a mortar and pestle. The powder was added to the FaSSGF solution at the beginning of the dissolution under stirring. Samples of 1.0 mL were collected after 0, 0.0083, 0.017, 0.083, 0.17, 0.5, 1, 3, 6, 18, 24 and 36 h to record the complete dissolution profile. The samples were placed in 5 mL volumetric flasks and completed to volume with FaSSGF. The absorbance was measured at a λ_{max} = 208 nm against a reagent blank in a 400-200 nm scan range using an Agilent Technologies Cary Series UV-Vis spectrophotometer, Cary 100 UV-Vis mode and the UV Cary Scan software (version v.20.0.470).

Figures S7.4-S7.5 depict the absorption spectra with the respective calibration curve for the ZOLE quantification in FaSSGF.

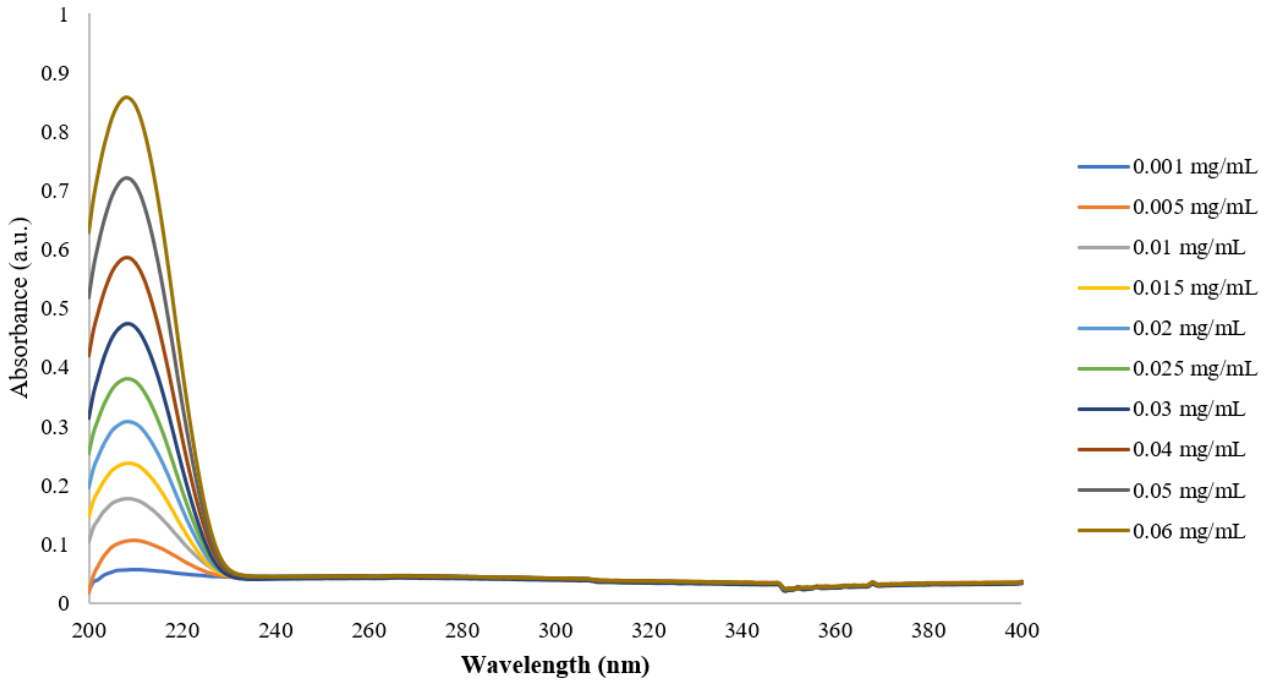

Figure S7.4. Absorbance spectra of ZOLE presenting a λ_{max} at 208 nm in FaSSGF in the concentration range of 0.001-0.06 mg/mL employed to construct a calibration curve.

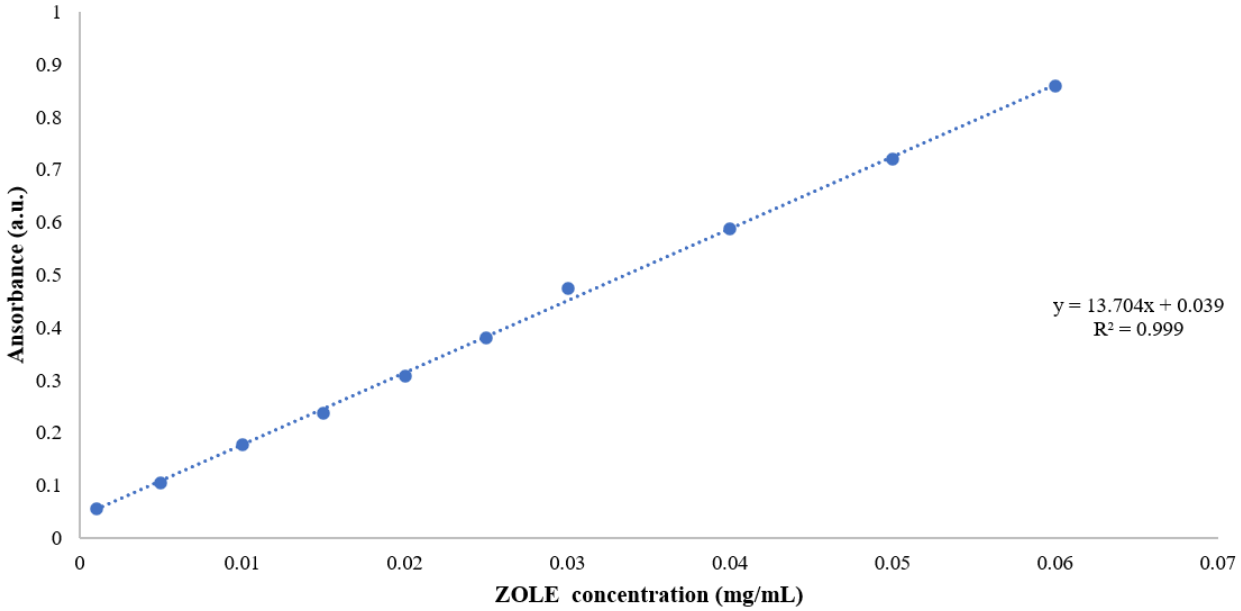

Figure S7.5. Calibration curve for ZOLE quantification for ZOLE-based BPCCs in FaSSGF.

9. Nanoemulsion Synthesis and Characterization of *nano*-Ca@ZOLE

9.1. Phase Inversion Temperature (PIT) Determination

A solution of ZOLE with a concentration of 2.5 mg/mL was prepared with nanopure water. In a 20 mL vial, 11 mL of the ZOLE solution was added with 3 mL of heptane and 0.9 mL of Brij® L4. The mixture was homogenized with an IKA T10 Basic Ultra Turrax (IKA Works Inc., Wilmington, NC), for 30 sec at a speed of "4" (14,450 rpm equivalent). The experimental set up was assembled using a jacketed beaker with a 20.3 cm (8") stainless steel RTD temperature probe (VWR®, VWR International). The conductivity of the content was measured with a Fisherbrand Accumet BasicAB30 conductivity meter (Fisher Scientific, Loughborough, UK). The bath temperature was controlled with a Julabo F32-ME Refrigerated/Heating Circulator (JULABO GmbH, Seelbach, Germany). Both the vial and the bath contained stir bars stirring at 300 rpm using a VWR® Professional Hot Plate Stirrer (97042-714, VWR®, VWR International). The internal temperature of the emulsion was allowed to reach 2.0°C in the bath before starting the measurements. A temperature profile cover the range from 2 and 40°C employing a heating rate of 1°C/min. The conductivity measurements were recorded in 1-degree intervals for the mixture. Figure S8.1 depicts the PIT determination curve for an aqueous ZOLE solution in heptane and Brij L4®.

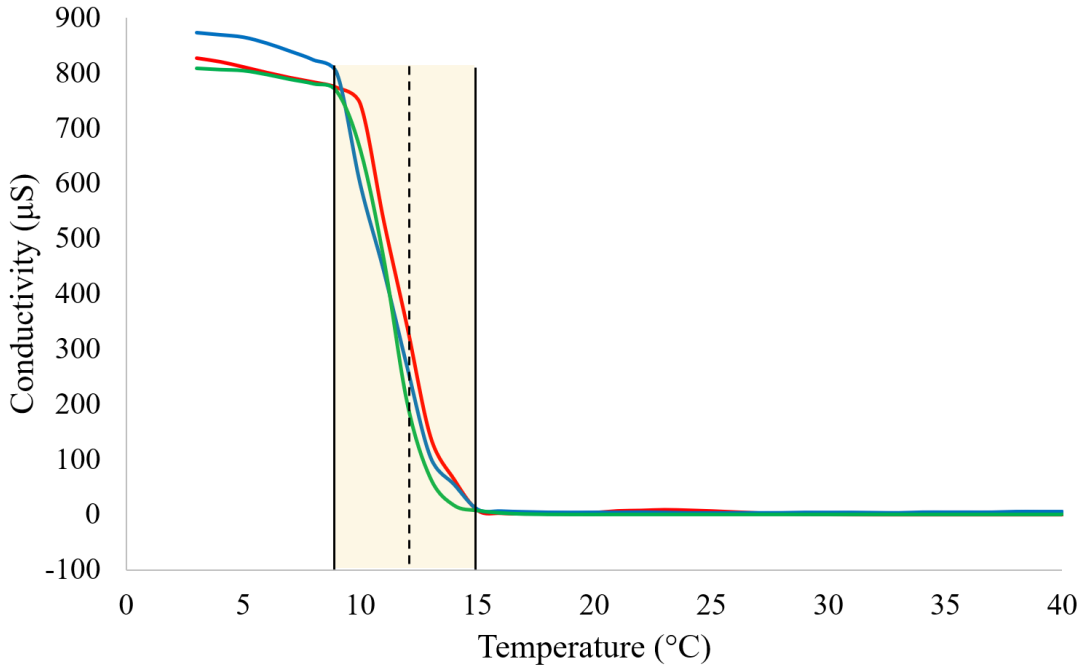

Figure S8.1. Nanoemulsion PIT determination of an emulsion containing ZOLE in water, heptane and Brij L4®, showing that the phase inversion occurs at approximately ~ 12°C (dashed line). Phase inversion starts at 9°C and ends at 15°C as depicted by the light orange region.

9.2. Nanoemulsion Synthesis of *nano*-Ca@ZOLE

The nanoemulsion synthesis was conducted in a Crystalline (Technobis Crystallization Systems, Alkmaar, Netherlands). The pre-homogenized emulsions prepared for the PIT determinations were used for the *nano*-Ca@ZOLE nanoemulsion synthesis. The emulsion was homogenized before being transferred to the reaction vial. From this mixture, 2.5 mL were transferred to a Crystalline reaction vial with a stir bar, sealed with a reflux cap. The vial was placed in the first reactor at 5°C for 30 min under 1,250 rpm continuous stirring. The vial was transferred to the second reactor at 45°C, where the emulsion was stirred for 30 min at 1,250 rpm before heating to 85°C. The metal salt solution was prepared dissolving 0.09 mmol (0.0135 g) of $CaCl_2 \cdot 2H_2O$ in 2.5 mL of nanopure water. The metal salt solution was added to the reaction vial via syringe after reaching 85°C. The solution was allowed to continue stirring at 1,250 rpm for 30 min at 85°C. Once the reaction completed, the reaction vial was left undisturbed for 1 h before analyzing the supernatant from the water phase.

Aliquots of the supernatant from the water phase presumed to contain *nano*-Ca@ZOLE nanoparticles were analyzed in a Malvern Panalytical Zetasizer NanoZS (Spectris PLC, Surrey, England) equipped with a He-Ne orange laser (633 nm, max 4 mW). Data was analyzed with Malvern software, version 7.12. The Zetasizer software automatically optimizes the built-in attenuator distance and the number of runs per measurement. The amount of run time was held constant at 10 sec, each measurement was performed in triplicate. The refractive index used for the sample was 1.333, which correspond to ZOLE in water. This value was determined by measuring an aliquot of 2.5 mg/mL ZOLE stock solution with a Mettler Toledo Refracto 30GS (Mettler Toledo, Columbus, OH).

9.3. Particle Size Distribution of *nano*-Ca@ZOLE Nanoparticles (after synthesis)

Aliquots of 50 µL of the supernatant from the water phase were transferred in disposable polystyrol/polystyrene cuvettes (REF: 67.754, 10 x 10 x 45 mm, Sarsted, Germany) in a 1:20 dilution ratio with 10% fetal bovine serum in PBS (10%FBS:PBS). The prepared samples remained undisturbed near the Zetasizer for 30 min prior to the measurements. Size measurements were performed after 2 min of sample equilibration inside the instrument at room temperature (25°C).

Tables S9.3.1-S9.3.3 summarize the DLS parameters and values after analyzing three PIT-nanoemulsion synthesis products in 10% FBS:PBS. Figures S9.3.1-S9.3.3 depict the DLS spectra showing the particle size distribution of the synthesized *nano*-Ca@ZOLE from the three synthesis attempts.

Table S9.3.1. Dynamic light scattering parameters and values after analyzing the PIT-nanoemulsion synthesis product.

PIT-Nanoemulsion synthesis No. 1				
Run	Size (d.nm)	% Intensity	St Dev (d.nm)	PDI
1	148.1	100.0	61.80	0.206
	0.000	0.0	0.000	
	0.000	0.0	0.000	
2	142.7	100.0	57.58	0.192
	0.000	0.0	0.000	
	0.000	0.0	0.000	
3	148.2	100.0	65.08	0.210
	0.000	0.0	0.000	
	0.000	0.0	0.000	
Average	146.3	100.0	61.62	0.202
	0.000	0.0	0.000	
	0.000	0.0	0.000	

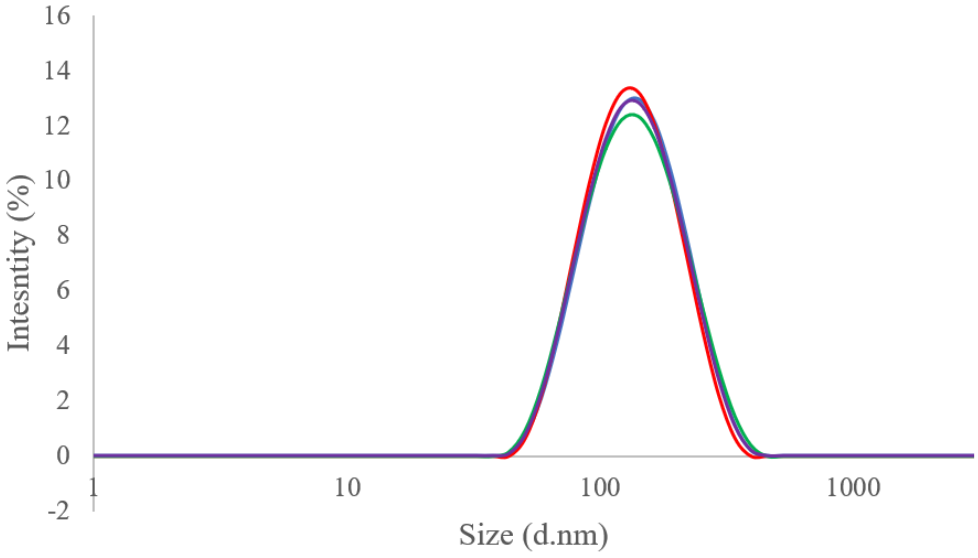

Figure S9.3.1. DLS spectra showing particle size distribution (d. nm) for each run (red, blue and green) and an average of 146.3 d.nm (purple).

Table S9.3.2. Dynamic light scattering parameters and values after analyzing the PIT-nanoemulsion synthesis product.

PIT-Nanoemulsion synthesis No. 2				
Run	Size (d.nm)	% Intensity	St Dev (d.nm)	PDI
1	156.3	100.0	73.84	0.203
	0.000	0.0	0.000	
	0.000	0.0	0.000	
2	157.9	100.0	75.70	0.210
	0.000	0.0	0.000	
	0.000	0.0	0.000	
3	151.3	100.0	59.44	0.194
	0.000	0.0	0.000	
	0.000	0.0	0.000	
Average	155.2	100.0	70.09	0.202
	0.000	0.0	0.000	
	0.000	0.0	0.000	

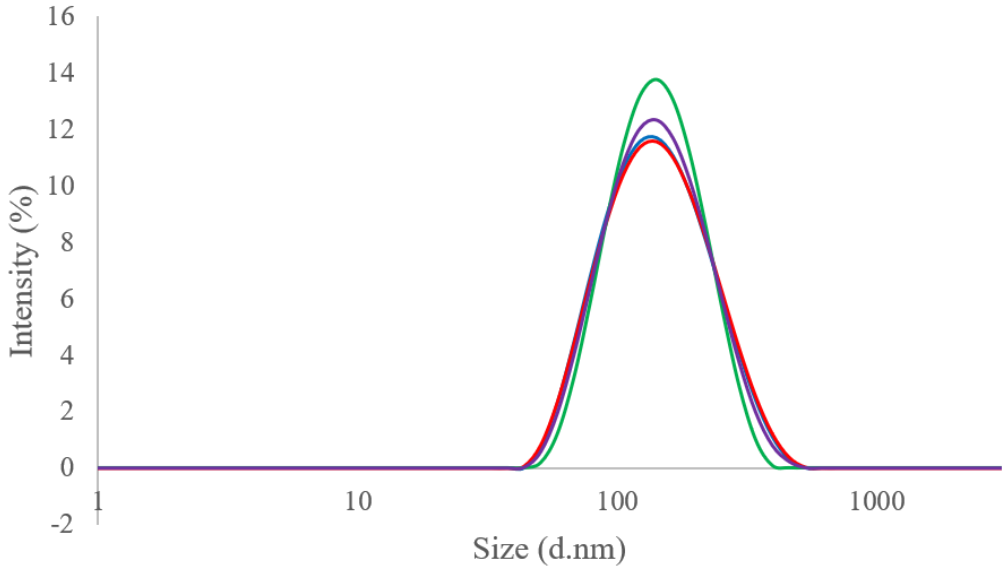

Figure S9.3.2. DLS spectra showing particle size distribution (d. nm) for each run (red, blue and green) and an average of 155.2 d.nm (purple).

Table S9.3.3. Dynamic light scattering parameters and values after analyzing the PIT-nanoemulsion synthesis product.

PIT-Nanoemulsion synthesis No. 3				
Run	Size (d.nm)	% Intensity	St Dev (d.nm)	PDI
1	145.8	100.0	71.19	0.207
	0.000	0.0	0.000	
	0.000	0.0	0.000	
2	142.2	100.0	59.95	0.196
	0.000	0.0	0.000	
	0.000	0.0	0.000	
3	145.1	100.0	63.10	0.215
	0.000	0.0	0.000	
	0.000	0.0	0.000	
Average	144.4	100.0	65.16	0.206
	0.000	0.0	0.000	
	0.000	0.0	0.000	

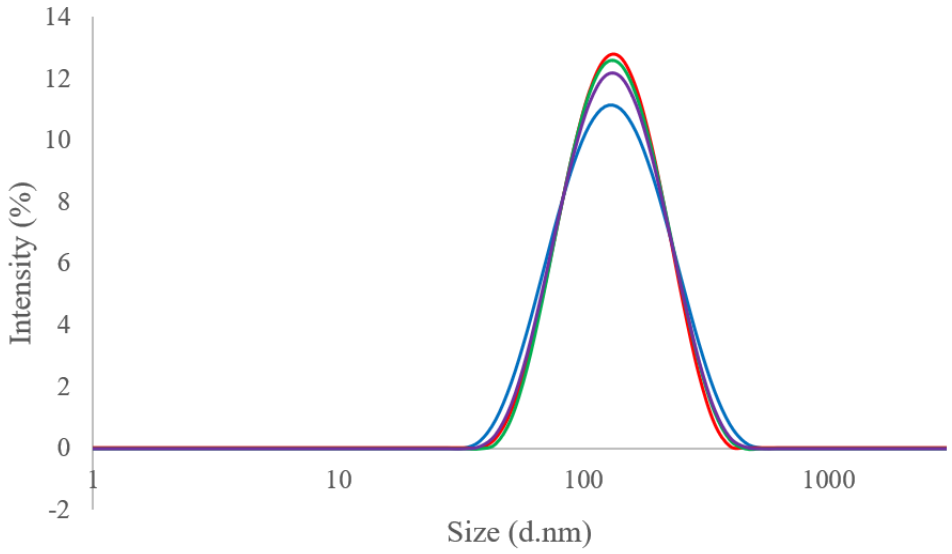

Figure S9.3.3. DLS spectra showing particle size distribution (d. nm) for each run (red, blue and green) and an average of 144.4 d.nm (purple).

9.4. Aggregation Measurements of *nano*-Ca@ZOLE in Biorelevant Dispersant

Aliquots of 50 μL of the supernatant from the water phase were transferred in disposable polystyrol/polystyrene cuvettes (REF: 67.754, 10 x 10 x 45 mm, Sarsted, Germany) in a 1:20 dilution ratio with 10% fetal bovine serum in PBS (10%FBS:PBS). The prepared samples remained undisturbed near the Zetasizer for 30 min prior to the measurements. Size measurements were performed in the biorelevant dispersant after 0, 24 and 48 h of sample preparation. Sample equilibration inside the instrument at room temperature (25°C) was performed for 2 min before measurements.

Tables S9.4.1-S9.4.3 summarize the DLS parameters and values after analyzing the *nano*-Ca@ZOLE in 10% FBS:PBS, at 0, 24 and 48 h. Figures S9.4.1-S9.4.3 depict the DLS spectra showing the particle size distribution of the synthesized *nano*-Ca@ZOLE in 10% FBS:PBS at the respective time points.

Aggregation tendency in <u>10% FBS:PBS</u>

Particle size distribution after 0 hours

Table S9.4.1. Dynamic light scattering parameters and values after analyzing the *nano*-Ca@ZOLE in 10% FBS:PBS after 0 h.

Particle size distribution: 10% FBS:PBS (0 h)				
Run	Size (d.nm)	% Intensity	St Dev (d.nm)	PDI
1	138.2	100.0	51.52	0.124
	0.000	0.0	0.000	
	0.000	0.0	0.000	
2	135.4	100.0	42.16	0.107
	0.000	0.0	0.000	
	0.000	0.0	0.000	
3	138.5	100.0	50.63	0.135
	0.000	0.0	0.000	
	0.000	0.0	0.000	
Average	137.4	100.0	48.31	0.122
	0.000	0.0	0.000	
	0.000	0.0	0.000	

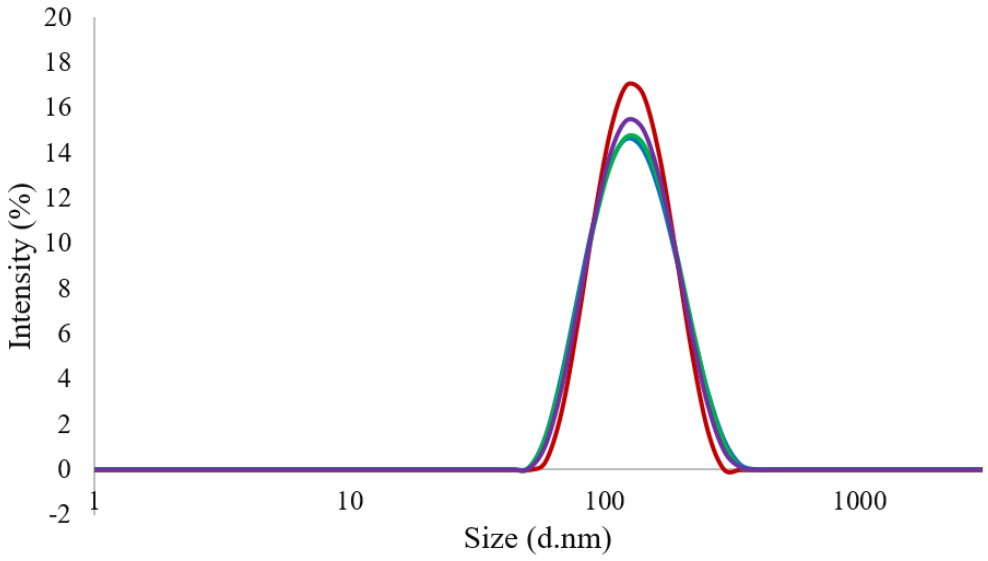

Figure S9.4.1. DLS spectra showing particle size distribution (d. nm) for each run (red, blue and green) and an average of 137.4 d.nm (purple).

Particle size distribution after 24 hours

Table S9.4.2. Dynamic light scattering parameters and values after analyzing the *nano*-Ca@ZOLE in 10% FBS:PBS after 24 h.

Particle size distribution: 10% FBS:PBS (24 h)				
Run	Size (d.nm)	% Intensity	St Dev (d.nm)	PDI
1	174.5	100.0	64.08	0.135
	0.000	0.0	0.000	
	0.000	0.0	0.000	
2	173.1	100.0	62.19	0.144
	0.000	0.0	0.000	
	0.000	0.0	0.000	
3	179.1	100.0	77.75	0.183
	0.000	0.0	0.000	
	0.000	0.0	0.000	
Average	175.5	100.0	68.41	0.154
	0.000	0.0	0.000	
	0.000	0.0	0.000	

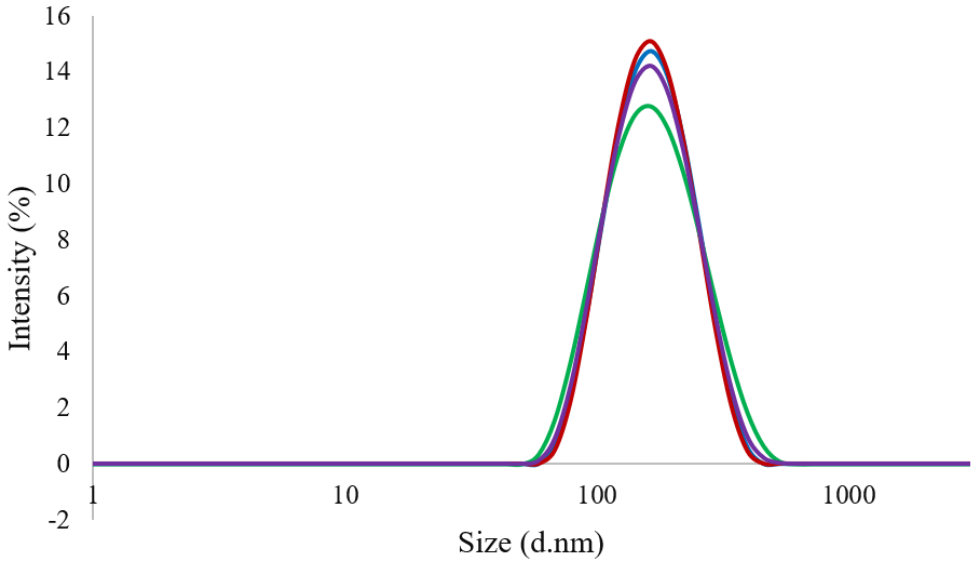

Figure S9.4.2. DLS spectra showing particle size distribution (d. nm) for each run (red, blue and green) and an average of 175.5 d.nm (purple).

Particle size distribution after 48 hours

Table S9.4.3. Dynamic light scattering parameters and values after analyzing the *nano*-Ca@ZOLE in 10% FBS:PBS after 48 h.

Particle size distribution: 10% FBS:PBS (48 h)				
Run	Size (d.nm)	% Intensity	St Dev (d.nm)	PDI
1	177.6	100.0	74.93	0.152
	0.000	0.0	0.000	
	0.000	0.0	0.000	
2	176.1	100.0	75.72	0.155
	0.000	0.0	0.000	
	0.000	0.0	0.000	
3	177.0	100.0	84.08	0.171
	0.000	0.0	0.000	
	0.000	0.0	0.000	
Average	176.9	100.0	78.36	0.159
	0.000	0.0	0.000	
	0.000	0.0	0.000	

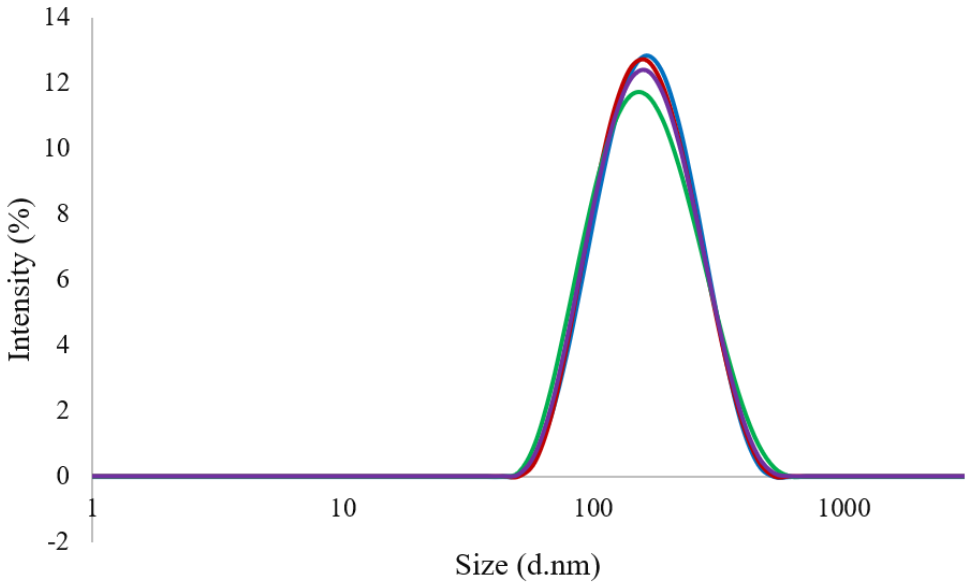

Figure S9.4.3. DLS spectra showing particle size distribution (d. nm) for each run (red, blue and green) and an average of 176.9 d.nm (purple).

9.5. Polarized Optical Microscopy/Powder X-ray Diffraction (*nano*-Ca@ZOLE)

Agglomerated nanocrystals of *nano*-Ca@ZOLE were mounted in 30 μm MiTeGen micro loop. Optical micrographs were recorded with a Nikon Eclipse Microscope LV100NPOL, equipped with a Nikon DS-Fi2 camera and NIS Elements BR software version 4.30.01. Powder X-ray diffraction analysis parameters were maintained the same as in *Section 3*. Figure S9.5.1 shows the representative sample mounted in the micro loop. Figure S9.5.2 depicts the PXRD overlay of ZOLE, ZOLE-Ca form II simulated pattern, ZOLE-Ca form II bulk crystals and *nano*-Ca@ZOLE nanocrystals.

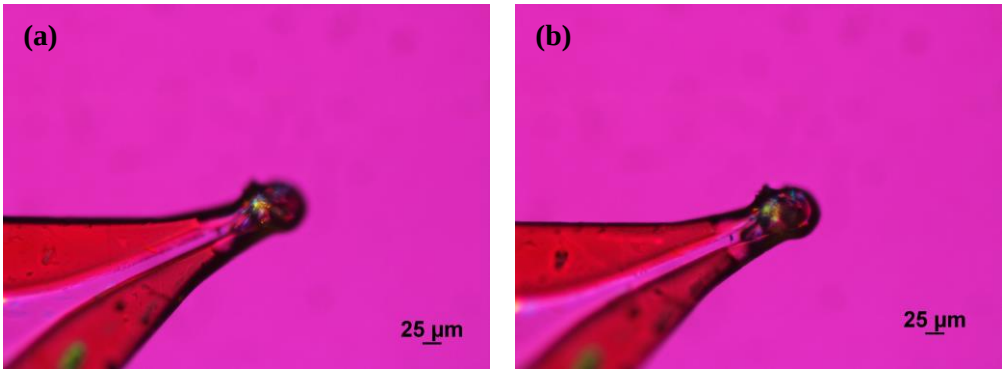

Figure S9.5.1. Polarized optical micrographs of *nano*-Ca@ZOLE agglomerated nanocrystals mounted in a 30 μm MiTeGen micro loop, observed at (a, b) 25*x* magnification.

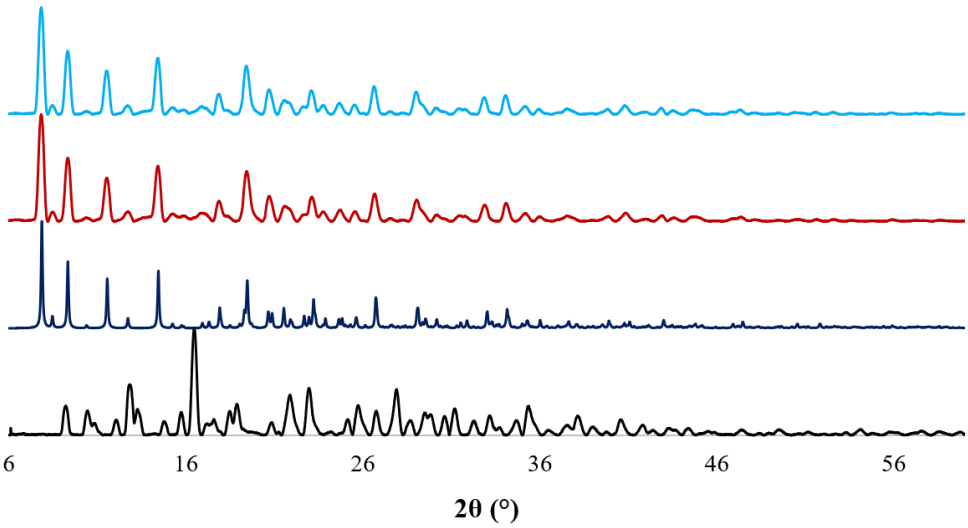

Figure S9.5.2. Powder X-ray diffractogram overlay of "as received" ZOLE (black), ZOLE-Ca form II simulated powder pattern (navy blue), ZOLE-Ca form II bulk crystals (red), and *nano*-Ca@ZOLE nanocrystals (light blue).

9.6. Binding Assays of *nano*-Ca@ZOLE to HA

Hydroxyapatite (HA) assay. For the *nano*-Ca@ZOLE binding assay, 20 mg of hydroxyapatite (HA), were exposed to 3.00 mL of *nano*-Ca@ZOLE (0.5 mg/mL) in PBS solution at 300 rpm and 37°C. HA in PBS mixture, as well as the binding of ZOLE to HA, were used as control groups. For the experimental groups (HA-*nano*-Ca@ZOLE and HA-ZOLE), collection was performed in duplicate. The selected time points were: 1, 2, 3, 4, 5, 7, 8, 9, 10, and 11 days. After each time point, the supernatant was collected, centrifuged (1,500 rpm, 8 min), and absorbance measurements were performed at λ_{max} = 208 nm to determine the percentage of ZOLE from the *nano*-Ca@ZOLE bound to HA. Figures S9.6.1 and S9.6.2 illustrate the binding curves of ZOLE and *nano*-Ca@ZOLE to HA in PBS. Solid samples of HA, HA-ZOLE, and HA-*nano*-Ca@ZOLE were characterized by SEM-EDS.

Energy dispersive spectroscopy (EDS). EDS elemental analysis of HA, HA-ZOLE, and HA-*nano*-Ca@ZOLE were recorded with a JEOL JSM-6480LV scanning electron microscope. The energy dispersive X-ray analysis (EDAX) Genesis 2000 detector was used to record the elemental composition of the samples.

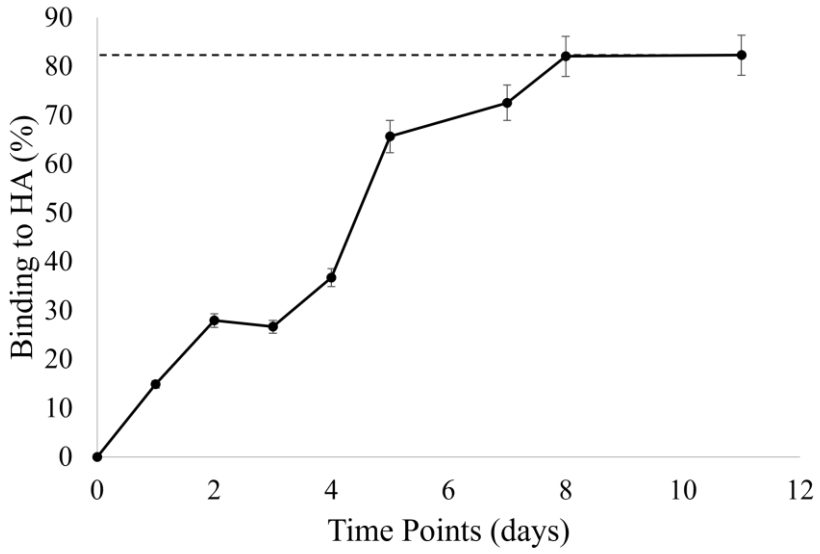

Figure S9.6.1. Binding curve of ZOLE to HA in PBS, reaching a maximum binding of 82% in 8 days (dashed line). Error bars for duplicate measurements fall below five percent (<5%) error.

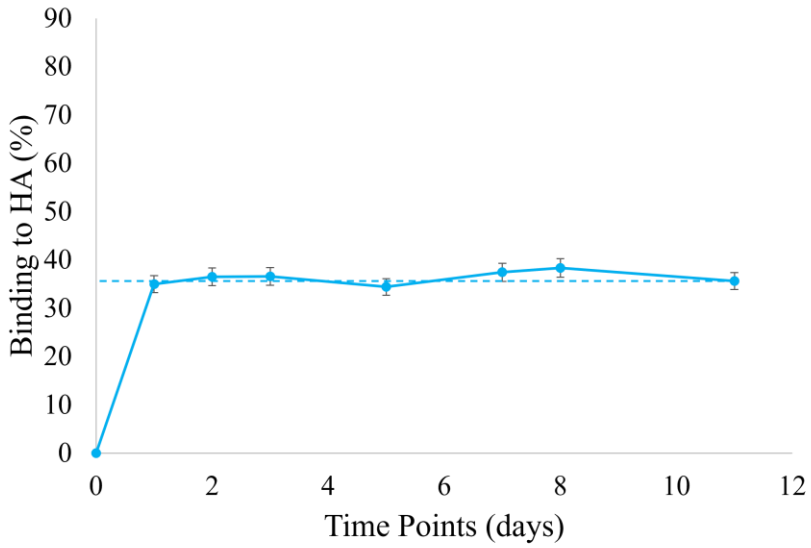

Figure S9.6.2. Binding curve of *nano*-Ca@ZOLE to HA in PBS, reaching a maximum binding of 36% in 1 day (dashed line). Error bars for duplicate measurements fall below five percent (<5%) error.

9.7. Cytotoxicity Assays for *nano*-Ca@ZOLE

Cell culture methods for the MDA-MB-231 cell line.[4] This cell line was grown in Dulbecco's Modified Eagle's Medium (DMEM) supplemented with 10 % fetal bovine serum (FBS) and 1 % penicillin-streptomycin (Pen-Strep), incubated at 37 °C and 5 % CO_2. Cell passage and cell treatment were performed at 80% of cell confluency. The completed growth media was exchanged every two days.

Cell culture methods for the hFOB 1.19 *cell line.*[5] This cell line was grown in 1:1 mixture of Ham's F12 Medium Dulbecco's Modified Eagle's Medium accompanied with 10 % FBS and 0.3 mg/ml of geneticin (G418), incubated at 34 °C in 5 % CO_2. Cell passage and cell treatment were performed at 80% of cell confluency. The completed growth media was exchanged every two days.

Cell seeding. The MDA-MB-231 and hFOB 1.19 cell lines were seeded in 96 well plates at a density of 2.5×10^5 cells/mL, incubation was carried out for 24 h at 37 °C for MDA-MB-231 and 34 °C for osteoblast hFOB 1.19, in 5% CO_2. The experiments were conducted in triplicates, three 96 well plates were made for each treatment period (24, 48, and 72 h).

Cell treatment. To determine the half-maximal inhibitory concentration (IC_{50}), for both cell lines, two-fold serial dilutions of ZOLE (0-200 µM) were prepared. To assess the relative cell live (%RCL) were employed selected two-fold serial dilutions (15, 7.5, 3.8, and 1.9 µM) of ZOLE and *nano*-Ca@ZOLE for MDA-MB-231 and hFOB 1.19 cell lines. For this, after the seeding, 100 µL of ZOLE and *nano*-Ca@ZOLE were used to treat the cells. The control groups were treated with just media. Both cell lines were incubated for 24, 48, and 72 h after ZOLE and *nano*-Ca@ZOLE solutions were added.

AlamarBlue® assay. For both cell lines, after the 24, 48, and 72 h of treatment, the media was removed from the 96 well plates. Subsequently, 100 µL of 10% AlamarBlue® solution was added and incubation was carried out for 4 h. The fluorescence (λ_{exc} = 570 nm, λ_{em} = 590 nm) was measured employing an Infinite M200 PRO Tecan Microplate Reader. The half-maximal effective concentration (IC_{50}) and the relative cell viability (%RCL) were assessed comparing the viability of the control group (100%) with the cells treated with the ZOLE and *nano*-Ca@ZOLE solutions. The IC_{50} curves and the %RCL values were plotted using the Graph Pad Prism 8 program.

Figure S9.7.1-S9.7.2 shows the IC_{50} curves for MDA-MB-231 and hFOB 1.19 treated with ZOLE (0-200 µM). The percentage of relative cell live (%RCL) for MDA-MB-231 and hFOB

1.19 cell lines using ZOLE and nano-Ca@ZOLE in concentrations of 1.9, 3.8, 7.5, and 15 µM are shown is Figures S9.7.3-S9.7.8.

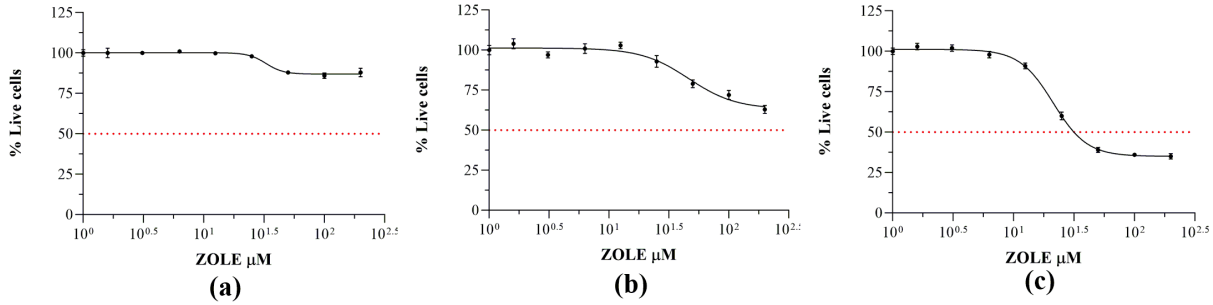

Figure S9.7.1. IC_{50} curves for ZOLE employing the human breast cancer MDA-MB-231 cell line at (a) 24, (b) 48, (c) 72 h of treatment.

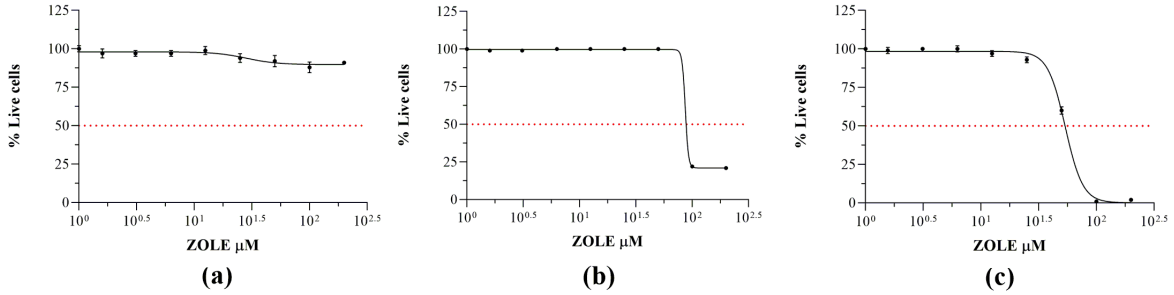

Figure S9.7.2. IC_{50} curves for ZOLE employing the osteoblast-like hFOB 1.19 cell line at (a) 24, (b) 48, (c) 72 h of treatment.

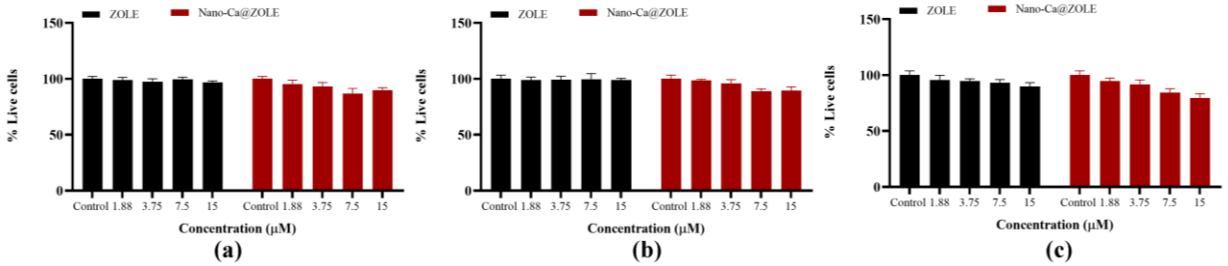

Figure S9.7.3. The relative cell live percentage (%RCL) of human breast cancer MDA-MB-231 cell line treated with ZOLE (black) and *nano*-Ca@ZOLE (red) at concentrations of 1.9, 3.8, 7.5, and 15 µM for 24 h.

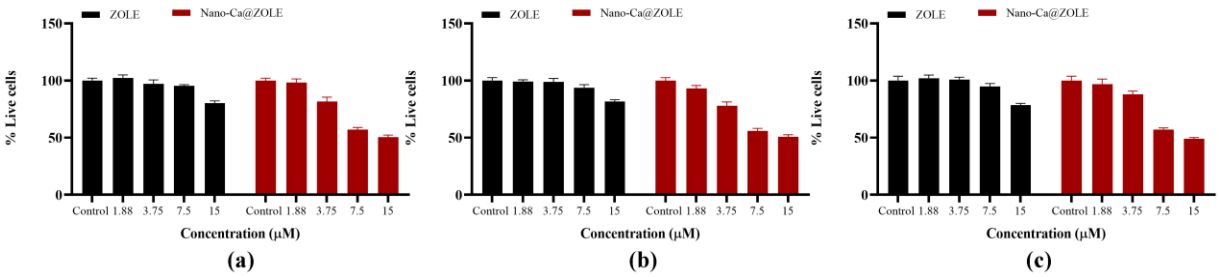

Figure S9.7.4. The relative cell live percentage (%RCL) of human breast cancer MDA-MB-231 cell line treated with ZOLE (black) and *nano*-Ca@ZOLE (red) at concentrations of 1.9, 3.8, 7.5, and 15 μM for 48 h.

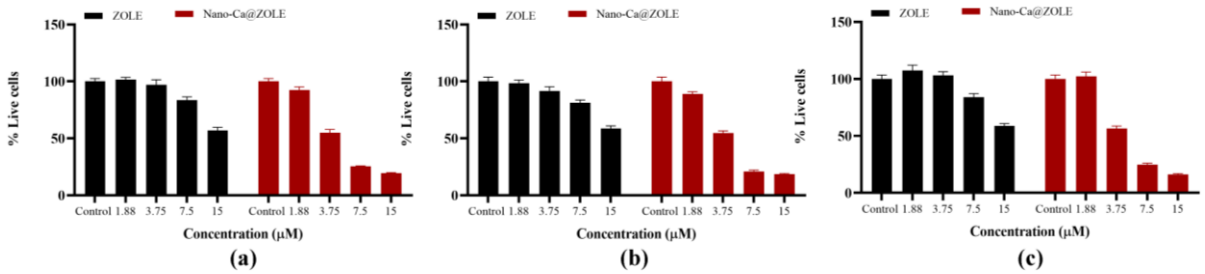

Figure S9.7.5. The relative cell live percentage (%RCL) of human breast cancer MDA-MB-231 cell line treated with ZOLE (black) and *nano*-Ca@ZOLE (red) at concentrations of 1.9, 3.8, 7.5, and 15 μM for 72 h.

Table S9.7.1. Relative cell viability (%) of MDA-MD-231 cell line treated with ZOLE and *nano*-Ca@ZOLE at 1.9, 3.8, 7.5, and 15 μM after 24, 48 and 72 h of treatment.

Time Points	1.9 μM		3.8 μM		7.5 μM		15 μM	
	ZOLE	*Nano*-Ca@ZOLE	ZOLE	*Nano*-Ca@ZOLE	ZOLE	*Nano*-Ca@ZOLE	ZOLE	*Nano*-Ca@ZOLE
Control	100	100	100	100	100	100	100	100
24 h	98 ± 2	96 ± 2	97 ± 2	94 ± 2	97 ± 4	87 ± 2	95 ± 5	86 ± 6
48 h	101 ± 2	96 ± 3	99 ± 2	83 ± 5	95 ± 1	57 ± 1	80 ± 2	50 ± 1
72 h	102 ± 5	94 ± 7	97 ± 6	55 ± 1	83 ± 1	24 ± 2	58 ± 1	18 ±2

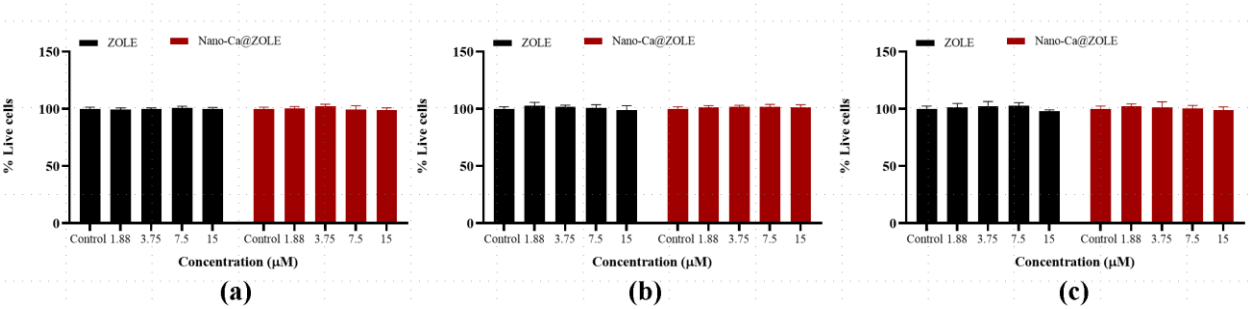

Figure S9.7.6. The relative cell live percentage (%RCL) of osteoblast hFOB 1.19 cell line treated with ZOLE (black) and *nano*-Ca@ZOLE (red) at concentrations of 1.9, 3.8, 7.5, and 15 μM for 24 h.

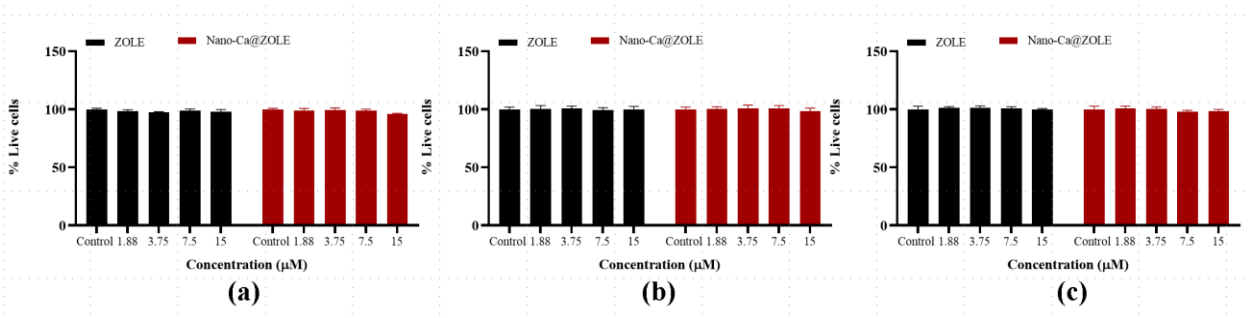

Figure S9.7.7. The relative cell live percentage (%RCL) of osteoblast hFOB 1.19 cell line treated with ZOLE (black) and *nano*-Ca@ZOLE (red) at concentrations of 1.9, 3.8, 7.5, and 15 μM for 48 h.

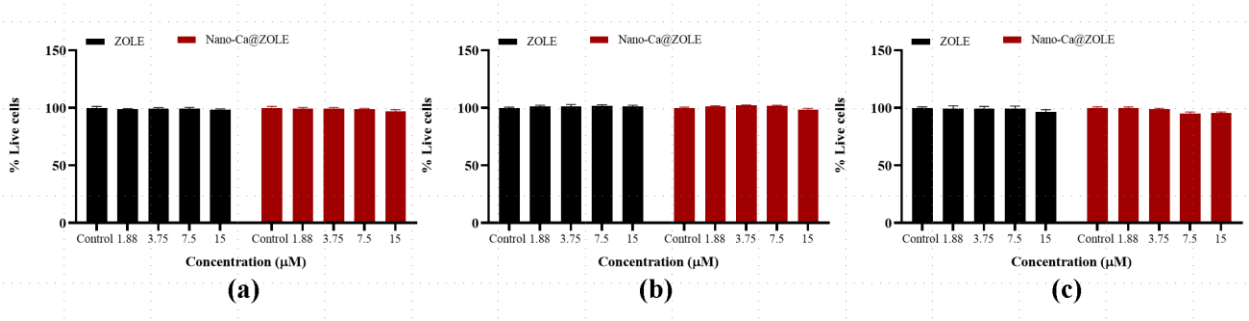

Figure S9.7.8. The relative cell live percentage (%RCL) of osteoblast hFOB 1.19 cell line treated with ZOLE (black) and *nano*-Ca@ZOLE (red) at concentrations of 1.9, 3.8, 7.5, and 15 μM for 72 h.

Table S9.7.2. Relative cell viability (%) of hFOB 1.19 cell line treated with ZOLE and *nano*-Ca@ZOLE at 1.9, 3.8, 7.5, and 15 μM after 24, 48 and 72 h of treatment.

Time Points	1.9 μM		3.8 μM		7.5 μM		15 μM	
	ZOLE	*Nano*-Ca@ZOLE	ZOLE	*Nano*-Ca@ZOLE	ZOLE	*Nano*-Ca@ZOLE	ZOLE	*Nano*-Ca@ZOLE
Control	100	100	100	100	100	100	100	100
24 h	101 ± 2	100 ± 1	101 ± 1	100 ± 1	101 ± 1	100 ± 1	99 ± 1	100 ± 1
48 h	100 ± 1	100 ± 1	100 ± 2	100 ± 1	100 ± 1	99 ± 1	99 ± 1	98 ± 1
72 h	100 ± 1	100 ± 1	100 ± 1	100 ± 2	100 ± 1	99 ± 3	99 ± 2	97 ± 2

10. References

(1) Freire, E.; Vega, D. R.; Baggio, R. Zoledronate Complexes. III. Two Zoledronate Complexes with Alkaline Earth Metals: [Mg(C5H9N2O7P 2)2(H2O)2] and [Ca(C 5H8N2O7P2)(H 2O)]N. *Acta Crystallogr. Sect. C Cryst. Struct. Commun.* **2010**, *66* (6). https://doi.org/10.1107/S0108270110017634.

(2) Cao, D. K.; Li, Y. Z.; Zheng, L. M. Layered Cobalt(II) and Nickel(II) Diphosphonates Showing Canted Antiferromagnetism and Slow Relaxation Behavior. *Inorg. Chem.* **2007**, *46* (18), 7571–7578. https://doi.org/10.1021/ic701098t.

(3) Zhang, Z. C.; Li, R. Q.; Zhang, Y. Diaquabis{[1-Hydr-Oxy-2-(1H-Imidazol-3-Ium-1-Yl)Ethane-1,1-Di-Yl] Bis-(Hydrogen Phospho-Nato)}manganese(II). *Acta Crystallogr. Sect. E Struct. Reports Online* **2009**, *65* (12). https://doi.org/10.1107/S160053680905065X.

(4) Freire, E.; Vega, D. R. Diaqua-Bis[1-Hydroxy-2-(Imidazol-3-Ium-1-Yl)-1,1′-Ethyl-Idenediphophonato-K2 O,O′]Zinc(II). *Acta Crystallogr. Sect. E Struct. Reports Online* **2009**, *65* (11). https://doi.org/10.1107/S1600536809042858.

(5) Freire, E.; Vega, D. R. Aquabis[1-Hydroxy-2-(Imidazol-3-Ium-1-Yl)-1,1′-Ethylidenediphophonato-K2 O,O′]Zinc(II) Dihydrate. *Acta Crystallogr. Sect. E Struct. Reports Online* **2009**, *65* (11). https://doi.org/10.1107/S160053680904286X.